
Masters Theses

Student Theses and Dissertations

Spring 2017

DC-DC converter based photovoltaic simulator with a double current mode controller

Weichao Zhang

Follow this and additional works at: https://scholarsmine.mst.edu/masters_theses



Part of the [Electrical and Computer Engineering Commons](#)

Department:

Recommended Citation

Zhang, Weichao, "DC-DC converter based photovoltaic simulator with a double current mode controller" (2017). *Masters Theses*. 7669.

https://scholarsmine.mst.edu/masters_theses/7669

This thesis is brought to you by Scholars' Mine, a service of the Missouri S&T Library and Learning Resources. This work is protected by U. S. Copyright Law. Unauthorized use including reproduction for redistribution requires the permission of the copyright holder. For more information, please contact scholarsmine@mst.edu.

**DC-DC CONVERTER BASED PHOTOVOLTAIC SIMULATOR
WITH A DOUBLE CURRENT MODE CONTROLLER**

by

WEICHAO ZHANG

A THESIS

**Presented to the Faculty of the Graduate School of the
MISSOURI UNIVERSITY OF SCIENCE AND TECHNOLOGY**

In Partial Fulfillment of the Requirements for the Degree

MASTER OF SCIENCE IN ELECTRICAL ENGINEERING

2017

Approved by

Jonathan W. Kimball, Advisor

Mehdi Ferdowsi

Pourya Shamsi

© 2017
Weichao Zhang
All Rights Reserve

ABSTRACT

This thesis presents the performance of a DC-DC converter based with current mode controller photovoltaic (PV) simulator which emulates the output characteristics of a real PV module. A portable PV simulator prototype of 85 W is examined in terms of its steady state IV curve matching capacity and the convergence time corresponding to step change in current source load, voltage source load, and insolation levels. The current-voltage (IV) characteristics of the PV module are implemented as a look-up-table (LUT) which determines the reference output current from measured output voltage. A Thevenin Equivalent Method approach to PV arrays analysis is also included in order to model the small-signal linearized characteristics. Extensive simulation results obtained in MATLAB are included to show that the PV simulator can work in most situations as a real PV module. Experimental results verify performance with current source and voltage source loads.

ACKNOWLEDGMENTS

I would like to thank my advisor Dr. Jonathan Kimball for his guidance and support which allow me to conduct this research. Without Dr. Kimball's vast knowledge and dedication in the electrical engineering field, this research will not come to fruition.

I would also like to acknowledge the members of my committee, Dr. Mehdi Ferdowsi and Dr. Pourya Shamsi, for their interest in my research topic and their instructions in electric drive machines and power electronics.

I would also like to thank my lab partners and friends for their helps and advises.

This project was supported in part by the National Science Foundation under awards 1505610 and 1406156. It was also supported in part by the MidAmerica Regional Microgrid Education and Training Consortium (MARMET), sponsored by the Department of Energy SunShot program under award DE0006341.

TABLE OF CONTENTS

	Page
ABSTRACT	iii
ACKNOWLEDGMENTS	iv
LIST OF ILLUSTRATIONS	vii
LIST OF TABLES	ix
NOMENCLATURE	x
SECTION	
1. INTRODUCTION	1
2. PV MODULE IV CURVE IMPLEMENTATION	3
2.1. PV MODULE MODELING	3
2.2. IV CURVE IMPLEMENTATION	5
3. CONTROLLER IMPLEMENTATION	11
3.1. DC-DC CONVERTER IMPLEMENTATION	11
3.2. CONVERTER SMALL SIGNAL MODELING	11
3.3. INNER PREDICTIVE CURRENT MODE CONTROLLER	13
3.4. OUTER PI CONTROLLER DESIGN	14
3.5. SYSTEM STABILITY ANALYSIS	16
4. SIMULATION RESULTS	18
5. HARDWARE IMPLEMENTATION	26
5.1. POWER STAGE OF THE PV SIMULATOR	26
5.2. INDUCTOR AND CAPACITOR SELECTION	27
5.3. THE DSP	29
6. EXPERIMENTAL RESULTS	30
6.1. PV SIMULATOR PROTOTYPE	30
7. CONCLUSION	38
7.1. RESEARCH FINDINGS	38
7.2. FUTURE WORK	38
APENDICES	
A. PRINTED CIRCUIT BOARD DESIGN	40

B. MATLAB CODE TO EXTRACT PV MODULE MODEL PARAMETERS	48
BIBLIOGRAPHY	52
VITA	54

LIST OF ILLUSTRATIONS

	Page
Figure 2.1. Equivalent circuit model of a PV cell	3
Figure 2.2. A PV module consists of series-connected PV cells.....	4
Figure 2.3. Thevenin Equivalent Circuit	6
Figure 2.4. Linearized IV curve under 100% insolation	7
Figure 2.5. IV curves of the PV module SW-S85P using equivalent circuit modeling.....	10
Figure 3.1. A synchronous buck converter.....	11
Figure 3.2. Control block diagram of the PV simulator	11
Figure 3.3. Mathematical building block of the converter operating in current mode control	14
Figure 3.4. PV module IV curve and gain.....	17
Figure 3.5. Bode plot of worst case system loop gain.....	17
Figure 4.1. Top level schematic of the PV simulator simulation model	18
Figure 4.2. Power stage simulation model of the PV simulator	19
Figure 4.3. Inside of “IV LUT” block	19
Figure 4.4. Control block simulation model for PV simulator.....	20
Figure 4.5. Computer simulated performance of the PV simulator	20
Figure 4.6. Computer Simulated output waveforms of the PV simulator when current source changes from 1A to 5A	21
Figure 4.7. Computer Simulated output waveforms of the PV simulator when voltage source changes from 20V to 16V	21
Figure 4.8. Computer Simulated insolation step change from 100% to 80% with current source load equals 3A	22
Figure 4.9. Computer Simulated insolation step change from 80% to 60% with current source load equals 3A	22
Figure 4.10. Computer Simulated insolation step change from 100% to 80% with current source load equals 2A	23
Figure 4.11. Computer Simulated insolation step change from 80% to 60% with current source load equals 2A	23
Figure 4.12. Computer Simulated insolation step change from 100% to 80% with voltage source load equals 20V	24

Figure 4.13. Computer Simulated insolation step change from 80% to 60% with voltage source load equals 20V	24
Figure 4.14. Computer Simulated insolation step change from 100% to 80% with voltage source load equals 19V	25
Figure 4.15. Computer Simulated insolation step change from 80% to 60% with voltage source load equals 19V	25
Figure 5.1. PV simulator hardware block diagram.....	26
Figure 5.2. Buck converter inductor current	28
Figure 6.1. PV simulator prototype built.....	30
Figure 6.2. PV simulator prototype's performance	32
Figure 6.3. Experiment setup for the PV simulator/PV module load dynamic response.....	33
Figure 6.4. Experimental insolation step change from 100% to 80% with current source load = 3A. Upper trace: voltage, 2.5 V/div; lower trace: current, 1.0 A/div; 100 μ s/div..	34
Figure 6.5. Experimental insolation step change from 100% to 80% with voltage source load = 20V. Upper trace: voltage, 2.5 V/div; lower trace: current, 1.0 A/div; 100 μ s/div..	34
Figure 6.6. Experimental output waveforms of the PV simulator when current source changes from 2A to 3A. Upper trace: voltage, 2.5 V/div; lower trace: current, 1.0 A/div; 20 ms/div..	35
Figure 6.7. Experimental output waveforms of the PV simulator when voltage source changes from 20V to 19V. Upper trace: voltage, 2.5 V/div; lower trace: current, 1.0 A/div; 20 μ s/div..	35
Figure 6.8. Theoretical, modeling, and measured closed-loop output impedances of buck converter in current source load. The red dashed line traces show the simulation results, the x line show the modeling output impedance, and the blue solid traces show the measured impedance.....	36
Figure 6.9. Theoretical, modeling, and measured closed-loop output impedances of buck converter in voltage source load. The red dashed line traces show the simulation results, the x line show the modeling output impedance, and the blue solid traces show the measured impedance.....	37

LIST OF TABLES

	Page
Table 6.1. PV Simulator Parameter	31
Table 6.2. PV Module Parameters	31

NOMENCLATURE

<u>Symbol</u>	<u>Description</u>
PV	Photovoltaic
MPPT	Maximum Power Point Tracking
LUT	Look-Up-Table
PWM	Pulse-Width Modulation
ADC	Analog-to-Digital Converter
PI	Proportional-Integral
DSP	Digital Signal Processor
I_D	Diode Current
V_D	Diode Voltage
I_0	Reverse Saturation Current
V_t	Thermal Voltage
A	Ideality Factor
k	Boltzmann's Constant
T	Absolute Temperature
q	Elementary Charge
I_{PVout}	Output Current of a PV Module
V_{PVout}	Output Voltage of a PV Module
R_s	Series Resistance of a PV Cell Model
R_{sh}	Shunt Resistance of a PV Cell Model
N	Number of Series Connected Cells of a PV Module
I_{ph}	Photo-generated Current
$I_{ph(max)}$	Photo-generated Current at Maximum Insolation
α	Insolation Percentage
A	Irradiance
MPP	Maximum Power Point
$V_{PVout}[i]$	Digital Output Voltage
V_{OC}	Open Circuit Voltage of a PV Module
A_{size}	Size of a Look-Up-Table

RAM	Random Access Memory
$I_{PVout}[i]$	Digital Output Reference Current
I_{SC}	Short Circuit Current of a PV Module
CCM	Continuous Conduction Mode
DCM	Discontinuous Conduction Mode
ESR	Equivalent Series Resistance
$G_{vd}(s)$	Small Signal Transfer Function Of Output Voltage Over Duty Ratio
$G_{id}(s)$	Small Signal Transfer Function Of Inductor Current Over Duty Ratio
$G_{iv}(s)$	Small Signal Transfer Function Of Output Current Over Output Voltage
L	Inductance
C	Capacitance
R_{ESR}	ESR of a Capacitor
R_L	DC Resistance of an Inductor
R	Load Resistance
$d[n+1]$	Predicted Duty Ratio for the Next Switch Cycle
$d[n]$	Duty Ratio for the Current Switch Cycle
$I_L[n]$	Measured Inductor Current
$I_{ref}[n]$	Reference Inductor Current for the Current Switch Cycle
T_s	Switching Period
$F_m(z)$	Predictive Current Mode Small Signal Transfer Function
$T(z)$	Discrete Time Loop Gain of the Plant
$G_{vd}(z)$	Discrete Time Equivalent of $G_{vd}(s)$
$G_{id}(z)$	Discrete Time Equivalent of $G_{id}(s)$
$G_{iv}(z)$	Discrete Time Equivalent of $G_{iv}(s)$
$F_m(s)$	Continuous Time Equivalent of $F_m(z)$
$G_c(s)$	Compensator
$G_c(z)$	Discrete Time Equivalent of $G_c(s)$
$T_{sys}(s)$	Loop Gain of Whole System
G_{LUT}	Small Signal Gain from LUT
V_{bat}	Input Battery Voltage
D_b	Boost Converter Duty Ratio

V_b	Output Voltage of Boost Converter
V_{out}	Output Voltage
D_{bk}	Buck Converter Duty Ratio
MOSFET	Metal Oxide Semiconductor Field Effect Transistor
ΔI_L	Peak-to-Peak Inductor Current Ripple
f_{sw}	Switching Frequency
ΔV_{out}	Peak-to-Peak Capacitor Voltage Ripple
PCB	Printed Circuit Board

1. INTRODUCTION

Solar energy has experienced phenomenal growth in recent years due to both technological improvements resulting in cost reductions and government policies supportive of renewable energy development and utilization. The most common way to harness solar energy is by converting it to electrical energy using photovoltaic (PV) modules. One challenge when interfacing devices to PV modules is that PV modules behave like a current source at high output current and a voltage source at low output current. This special output characteristic of PV modules requires devices that interface with them to have maximum power point tracking (MPPT) capabilities in order to maximize the efficiency of PV modules [1, 2]. Field testing MPPT converters with real PV modules is challenging. First, PV modules are still expensive despite the fact that their price has been on a steady decline over the past decade. Installation of PV modules is also an expensive and time-consuming process. Second, the output of PV modules is dependent on the insolation level and temperature, which varies depending on the time of year and weather of the day; hence test conditions cannot be controlled and repeatable test results cannot be obtained.

PV systems are unusual in that they cannot be turned on or off. That is, they produce voltage, possibly at dangerous levels, any time they are receiving sunlight. Another important point is PV panels generate dc voltage, which is not always commonly used by electricians in their normal work. In addition, because of the current limiting properties of PV cells, they are incapable of producing sufficient fault currents to operate over-current protection devices such as fuses. An alternative to field testing a PV system is to replace the PV module with a PV simulator, which is a device that has the same output characteristic of a real PV module, and can be used within a lab environment at any time of the year. The method used in this paper to simulate a real PV module is to digitally implement the current-voltage (IV) characteristic of a PV module through a look-up-table (LUT) that resides in the memory of the microcontroller and convert the digital signal to power output through a dc-dc converter [5-9]. The major advantage of digitally implemented PV simulators is that it provides a controlled environment where users can set conditions such as temperature, insolation level. Moreover, digital control of

a pulse-width modulation (PWM) converter has the advantage of high noise immunity, immunity to analog component variations, fast design process and programmability for multiple applications, as compared to an analog counterpart [10-12]. With digital control, more complex control schemes can be easily achieved, such as the double current mode controller described in the present work.

This work extends previous work [13] and uses a similar framework. However, the method in [13] was only demonstrated with resistive loads. When tested on other types of loads, for example, the current source and voltage source load, the converter became unstable. Therefore, a new approach is proposed here.

In Section II, the mathematical model of a PV module is derived and two methods to implement the mathematical model as a LUT are proposed. In Section III, the small signal transfer functions are derived, and the inner predictive current mode controller and the outer PI controller are designed to satisfy gain margin and phase margin requirements. Section IV includes both simulation results and experimental results that verify the operation of the controller.

2. PV MODULE IV CURVE IMPLEMENTATION

2.1. PV MODULE MODELING

A PV Cell can be modeled as a network that consists of a current source, a diode, a shunt resistor and a series resistor configured as shown in Fig. 2.1.

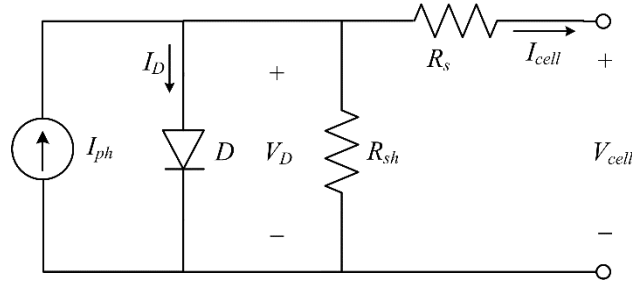


Figure 2.1. Equivalent circuit model of a PV cell

The diode equation is given as

$$I_D = I_0 \left(e^{\frac{V_D}{V_t}} - 1 \right) \quad (1)$$

$$V_t = \frac{AkT}{q} \quad (2)$$

where I_D is the current through the diode, V_D is the voltage across the diode, I_0 is reverse saturation current, V_t is thermal voltage, A is ideality factor, k is Boltzmann's constant, T is absolute temperature and q is elementary charge. A PV module is made of many series-connected PV cells as shown in Fig. 2.2. As a result, the voltage across each cell is the total output voltage of the PV module divided by the number of series-connected cells, and the current through each PV cell is the same as the output current of the PV module.

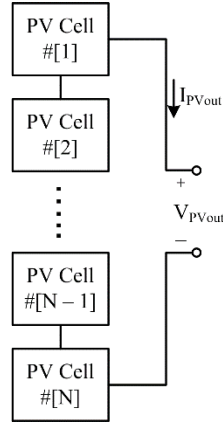


Figure 2.2. A PV module consists of series-connected PV cells

The output equation that relates the output current and output voltage of a PV module can be derived as

$$I_{PVout} = I_{ph} - I_0 \left(e^{\frac{V_{PVout} + I_{PVout} R_s}{N V_i}} - 1 \right) - \frac{V_{PVout} + I_{PVout} R_s}{R_{sh}} \quad (3)$$

$$I_{ph} = \alpha \cdot I_{ph(max)} \quad (4)$$

$$\alpha = \frac{\Lambda}{1000 \text{ W/m}^2} \quad (5)$$

where I_{PVout} is the output current of the PV module, V_{PVout} is the output voltage of the PV module, R_s is the series resistance of the PV cell model, R_{sh} is the shunt resistance of the PV cell model, N is the number of series-connected cells, I_{ph} is the photo-generated current which is proportional to the amount of insolation received by the PV module as shown in (4) and (5), $I_{ph(max)}$ is the photo-generated current at 100% insolation, and Λ is

the irradiance from the sun received by the PV module, which is normalized to standard test condition (STC) of 1000 W/m^2 to find α , the insolation percentage. From (1)-(3), the IV curve of a PV module is characterized by R_s , R_{sh} , N , I_{ph} , A , T and I_0 . By varying these parameters, one can model many different kinds of PV modules under different environmental conditions.

However, solar panel datasheets generally do not specify the parameters used in (3) explicitly, so these parameters must be extracted from other specified parameters from the datasheets. One technique requires only three values: the open circuit voltage, the short circuit current and the maximum power point (MPP) voltage and current [19]. The core of this technique involves stepping through all possible values of R_s and R_{sh} until the requirement that the derivative of power over voltage is zero is satisfied at the MPP. The Matlab¹ code to implement this technique is attached in Appendix B. The datasheet parameters and the extracted equivalent circuit model parameters have been compiled in Table 6.1 for the PV module SW-S85P from SunWize in Section 6.

2.2. IV CURVE IMPLEMENTATION

The PV module IV characteristic is represented by a LUT, which is updated whenever the controller receives a command to change the operating conditions, such as a different insolation level. In order to store the IV curve as a LUT in memory, a set number of matching output voltage and output current pairs has to be determined according to the Thevenin Equivalent Method based on (3). A Thevenin equivalent circuit shown in Fig. 2.3. is derived where the Thevenin equivalent voltage V_{th} and resistance R_{th} are depend on the operating conditions such as insolation and the load. When the insolation level and/or the load changes, the linear IV characteristics changes as well.

¹ Matlab is a registered trade mark of The Math Works, Inc.

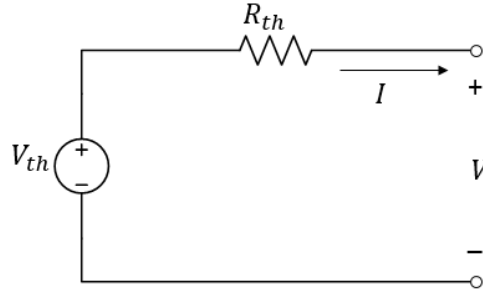


Figure 2.3 Thevenin Equivalent Circuit

In order to obtain the linear characteristics curves, the differentiated equation with respect to V of (6) is given as

$$\frac{dI}{dV} = -I_0 \frac{1 + R_s \frac{dI}{dV}}{NV_t A} e^{\frac{V + R_s I}{V_t A}} - \frac{1 + R_s \frac{dI}{dV}}{R_{sh}} \quad (6)$$

The Thevenin resistance, R_{th} , is the slope and can be derived as

$$-R_{th} = -R_s - \left(\frac{I_0}{AV_t} e^{\frac{V + R_s I}{AV_t}} + \frac{1}{R_{sh}} \right)^{-1} \quad (7)$$

Combining the slope with short circuit current, the linear I-V characteristics may be easily obtained. As a result, according to the maximum power transfer theorem [4], in order to extract the maximum available power from the solar array, a load equal to the Thevenin resistance must be introduced, satisfying

$$\frac{V}{I} = R_s + \left(\frac{I_0}{AV_t} e^{\frac{V + R_s I}{AV_t}} + \frac{1}{R_{sh}} \right)^{-1} \quad (8)$$

The LUT is a 1000-element, one dimensional array that stores the output currents corresponding to output voltages. Here the size of the array is limited by the random access memory (RAM) size of the microcontroller and can be increased if higher

resolution is necessary and RAM permits. The LUT is updated whenever the controller receives a command to change the operating conditions, such as a different insolation level. With a set number of matching output voltage and output current from PV module, a collection of linear characteristics is obtained in Simulink according to Thevenin Equivalent Theorem, as shown in Fig. 2.4. Each tangent line corresponding to a different load on the IV curve under a 100% insolation condition (MPP Load Line only shown). The MPP is reached when the absolute value of the slope equals the load resistance. The nonlinear IV curve is formed by the intersection of linear IV curve and the load line. This point is determined by different load resistance and its corresponding slope.

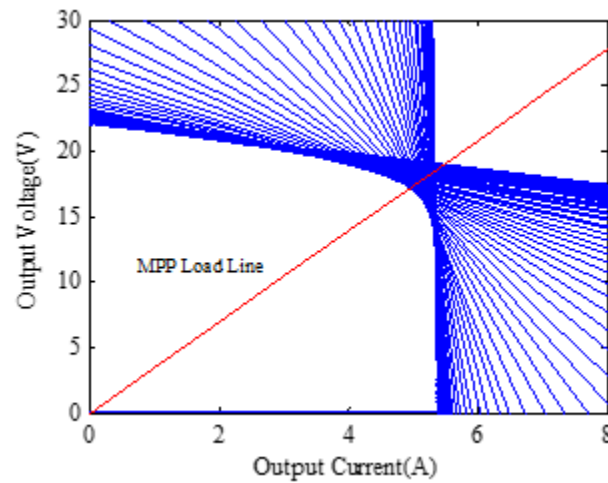


Figure 2.4 Linearized IV curve under 100% insolation

For the double current mode controller to be presented in this paper, an output current reference is generated according to a measured output voltage. For simplicity, the output voltage corresponding to the i^{th} element of the LUT is set as

$$V_{PVout}[i] = i \frac{V_{OC}}{A_{size}}, i = 0, 1, 2, \dots, (A_{size} - 1) \quad (6)$$

where V_{OC} is the open circuit voltage of the IV curve and A_{size} is the size of the LUT. A_{size} is limited by the random access memory (RAM) size of the microcontroller and can be

increased if higher resolution is necessary and RAM permits. The i^{th} element of the LUT, which contains the output current reference $I_{PVout}[i]$, can be calculated according to (3). However, (3) has no analytical solution because I_{PVout} is on both sides of the equation and in a transcendental function, so Newton's method is used to find the numeric solutions. Equation (3) can be rearranged into

$$f(I_{PVout}[i]) = I_{PVout}[i] - I_{ph} + I_0 \left(e^{\frac{\frac{V_{PVout}[i]}{N} + I_{PVout}[i] \cdot R_s}{V_t}} - 1 \right) + \frac{V_{PVout}[i] + I_{PVout}[i] \cdot R_s}{R_{sh}} \quad (7)$$

with the output current reference $I_{PVout}[i]$ as its independent variable. The i^{th} LUT entry is the root of $f(I_{PVout}[i])=0$. Newton's method is given as [20]

$$I_{PVout}[i][n+1] = I_{PVout}[i][n] - \frac{f(I_{PVout}[i][n])}{f'(I_{PVout}[i][n])} \quad (8)$$

where

$$f'(I_{PVout}[i][n]) = I_0 \left(e^{\frac{\frac{V_{PVout}[i]}{N} + I_{PVout}[i][n] \cdot R_s}{V_t}} \right) \frac{R_s}{V_t} + \frac{R_s}{R_{sh}} + 1 \quad (9)$$

$I_{PVout}[i][n+1]$ is the approximation to the real root of $f(I_{PVout}[i])=0$ after $n+1$ iterations. The initial guess $I_{PVout}[i][0]$ can be set to the short circuit current of the IV curve.

Once the array is filled up with voltage and current pairs, it may be used to represent the PV module. The index i to the array is calculated according to

$$i = \text{round}\left(A_{size} \frac{V_{out}}{V_{OC}}\right) \quad (10)$$

where V_{out} is the output voltage of the PV simulator.

Newton's method gives accurate solutions and only the output voltage is required to calculate the corresponding output current, which means only the output voltage needs to be measured to generate the index i . However, setting up the LUT requires a considerable amount of computing power from the microcontroller, which is a limited resource in embedded systems. This makes real time changes to the IV curve implausible due to large calculation delays.

Another technique to calculate the voltage and current pairs involves expressing the output current as a function of the diode voltage as

$$I_{PVout} = I_{ph} - I_0 \left(e^{\frac{V_D}{V_t}} - 1 \right) - \frac{V_D}{R_{sh}} \quad (11)$$

$$V_D = \frac{V_{PVout}}{N} + I_{PVout} R_s \quad (12)$$

V_D becomes the indexed voltage to the LUT, and its value corresponding to the i^{th} element of the LUT is set as

$$V_{out} = i \frac{\frac{V_{OC}}{N} + I_{SC} R_s}{A_{size}} \quad (13)$$

where I_{SC} is the short circuit current of the IV curve. Then $I_{PVout}[i]$ is calculated by

$$I_{PVout}[i] = I_{ph} - I_0 \left(e^{\frac{V_D[i]}{V_t}} - 1 \right) - \frac{V_D[i]}{R_{sh}} \quad (14)$$

The index i to the LUT is generated according to

$$i = \text{round}\left(A_{\text{size}} \frac{V_{\text{out}} + I_{\text{out}} R_s N}{V_{\text{OC}} + I_{\text{SC}} R_s N}\right) \quad (15)$$

One drawback of this technique is that it requires the knowledge of both the output voltage and output current, which requires an extra current sensor besides an output voltage sensor, to generate the index i . However, the extra current sensor is already in place because the output current is regulated. This method does not require iterations of Newton's method and therefore drastically reduces the calculation time required to setup the LUT. The implementation of the PV simulator described below incorporates the abilities to simulate real time insolation and temperature changes, which is achieved with the fast method of (11) to (15).

The IV curves of the PV module SW-S85P corresponding to 100%, 80%, 60%, 40% and 20% insolation levels along with their MPPs are shown in Fig. 2.5 with the diode voltage method. The same IV curves can also be obtained with Newton's method.

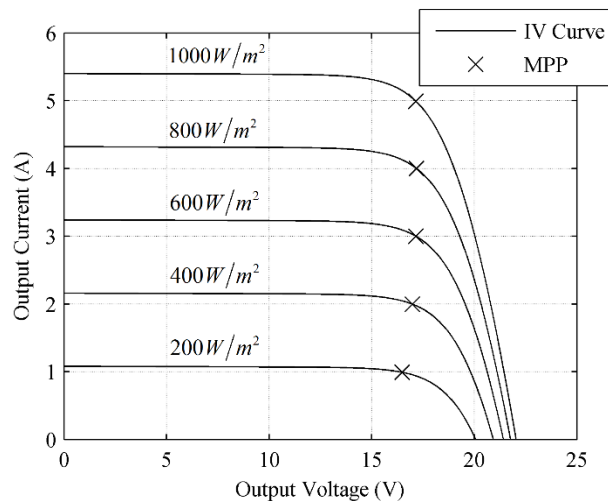


Figure 2.5. IV curves of the PV module SW-S85P using equivalent circuit modeling

3. CONTROLLER IMPLEMENTATION

3.1. DC-DC CONVERTER IMPLEMENTATION

To achieve a variable output voltage, a synchronous buck converter topology is utilized as shown in Fig. 3.1. This topology has high efficiency over a wide operating range, a key feature given the need to reach both short-circuit and open-circuit conditions.

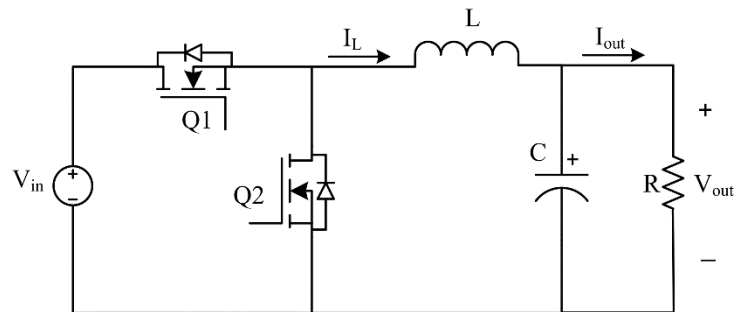


Figure 3.1. A synchronous buck converter

3.2. CONVERTER SMALL SIGNAL MODELING

The control block diagram is shown in Fig. 3.2. In order to design a controller for the simulator, the small signal transfer functions of the buck converter must be derived.

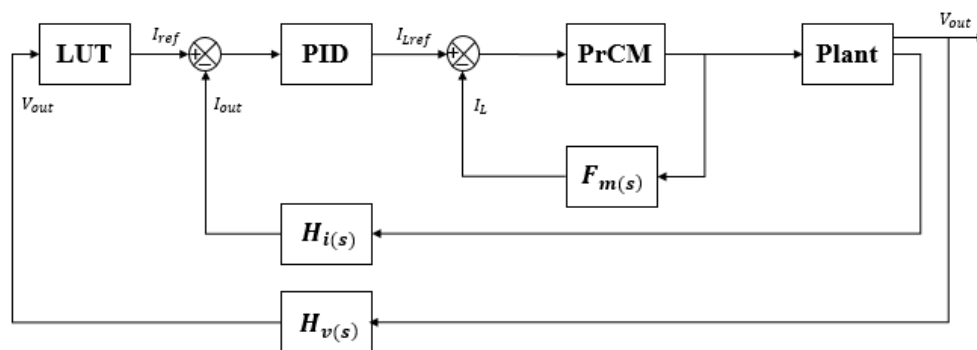


Figure 3.2. Control block diagram of the PV simulator

The control block diagram is shown in Fig. 3.2. In order to design a controller for the simulator, the small signal transfer functions of the buck converter must be derived.

Here only the small signal transfer functions for the buck converter operating in continuous conduction mode (CCM) are needed because the buck converter is synchronous and will never run into discontinuous conduction mode (DCM). These small signal transfer functions can be derived using averaged switch modeling or state space averaging; both methods produce the same transfer functions [21]. The process accounts for the inductor DC resistance and equivalent series resistance (ESR) of the capacitor. Assuming a pure resistive load and that the inductor DC resistance and the ESR of the capacitor are much less than the load resistance, the continuous time small signal transfer functions are derived as

$$\begin{aligned}
 G_{vd}(s) &= \left. \frac{\tilde{v}_{out}(s)}{\tilde{d}(s)} \right|_{\tilde{v}_{in}(s)=0} \\
 &= \frac{V_{in}R(1+CR_{esr} \cdot s)}{LC(R+R_{esr})s^2 + [L+CR_{esr}R_L + CR(R_{esr} + R_L)]s + R + R_L} \\
 &\approx \frac{V_{in}R(1+CR_{esr} \cdot s)}{LCR \cdot s^2 + [L+CR(R_L + R_{esr})]s + R + R_L} \tag{16}
 \end{aligned}$$

$$\begin{aligned}
 G_{id}(s) &= \left. \frac{\tilde{i}_L(s)}{\tilde{d}(s)} \right|_{\tilde{v}_{in}(s)=0} \\
 &= \frac{V_{in} [1 + C(R_{esr} + R)s]}{LC(R+R_{esr})s^2 + [L+CR_{esr}R_L + CR(R_{esr} + R_L)]s + R + R_L} \\
 &\approx \frac{V_{in} (1 + CR \cdot s)}{LCR \cdot s^2 + [L+CR(R_L + R_{esr})]s + R + R_L} \tag{17}
 \end{aligned}$$

$$G_{iv}(s) = \frac{\tilde{i}_{out}(s)}{\tilde{v}_{out}(s)} = \frac{1}{R} \quad (18)$$

where $G_{vd}(s)$ is the small signal transfer function of output voltage over duty ratio, $G_{id}(s)$ is the small signal transfer function of inductor current over duty ratio, $G_{iv}(s)$ is the small signal transfer function of output current over output voltage, L is the inductance, C is the capacitance, R_{ESR} is the ESR of the output capacitor, R_L is the DC resistance of the inductor, V_{in} is the input voltage, and R is the load resistance.

3.3. INNER PREDICTIVE CURRENT MODE CONTROLLER

Predictive current control is an accurate digital control technique that is based on inductor current predicted by sampled inductor current and output voltage. There are three kinds of predictive current mode controls – peak current control, average current control and valley current control. There are four kinds of modulation methods – trailing edge, leading edge, trailing triangle and leading triangle. Each of the three current control methods must be paired with the correct modulation method in order to be stable over the whole range of the duty ratio. Here average current control is used to increase noise immunity, and it is paired with trailing triangle modulation to give stability over the whole duty ratio range of the buck converter. Regardless of the current control method, the predictive current mode control law for a buck converter is given as [12]

$$d[n+1] = -d[n] + \frac{L}{V_{in}T_s} (I_{ref}[n] - I_L[n]) + \frac{2V_{out}}{V_{in}} \quad (19)$$

where $d[n+1]$ is the predicted duty ratio for the next switch cycle, $d[n]$ is the duty ratio of the current switch cycle, $I_L[n]$ is the measured inductor current for the current switch cycle, $I_{ref}[n]$ is the reference inductor current for the current switch cycle, and T_s is the switching period. The small signal discrete time transfer function of duty ratio over current error is given as [13]

$$d(z) = F_m(z)[I_{ref}(z) - I_L(z)] \quad (20)$$

where

$$F_m(z) = \frac{L}{V_{in} T_s} \frac{1}{z+1} \quad (21)$$

Fig. 3.3. illustrates the mathematical representation of the current mode controlled converter. The current modulator employed here is discussed in detail in [8]. The extra elements in this control scheme are R_{th} and F_m . The term R_{th} represents the current sensing resistor that transforms current to voltage to control the inductor current. The term F_m represents gain blocks related to the current modulator, and f_{sw} is the switching frequency and ma is the slope of artificial ramp.

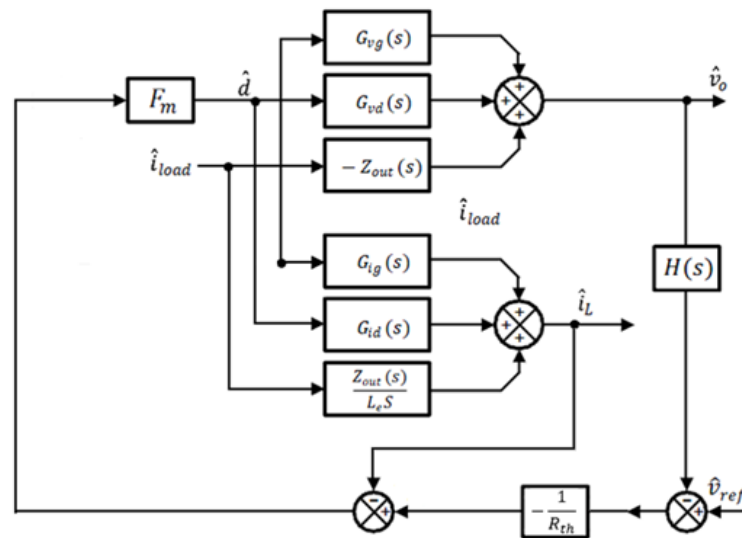


Figure 3.3 Mathematical building block of the converter operating in current mode control

3.4. OUTER PI CONTROLLER DESIGN

From the block diagram shown in Fig. 3.2, the discrete time loop gain of the plant without the compensator $G_c(z)$ can be found using loop reduction or Mason's Law.

Assuming that the gains from the ADCs have been adjusted to unity, the discrete time loop gain of the plant is found as

$$T(z) = \frac{F_m(z)G_{vd}(z)G_{iv}(z)}{1 + F_m(z)G_{id}(z)} \quad (22)$$

where $G_{vd}(z)$, $G_{id}(z)$ and $G_{iv}(z)$ are the discrete time equivalents of $G_{vd}(s)$, $G_{id}(s)$ and $G_{iv}(s)$ respectively. To design the compensator in the continuous time domain, the loop gain from (22) is converted to the continuous time domain by converting $F_m(z)$ to the continuous time domain $F_m(s)$ using bilinear transform as

$$F_m(s) = F_m(z) \left|_{\substack{z = \frac{1 + \frac{T_s}{2}s}{1 - \frac{T_s}{2}s}} = \frac{L \left(1 - \frac{T_s}{2}s\right)}{2T_s V_{in}} \quad (23)$$

Then the loop gain becomes

$$T(s) = \frac{F_m(s)G_{vd}(s)G_{iv}(s)}{1 + F_m(s)G_{id}(s)} = \frac{2L(1 + CR_{esr} \cdot s) \left(1 - \frac{T_s}{2}s\right)}{D(s)} \quad (24)$$

where

$$D(s) = 3CLRT_s \cdot s^2 + (4CRR_L T_s + 4CRR_{esr} T_s + 3LT_s + 2CLR)s + 2L + 4RT_s + 4R_L T_s \quad (25)$$

The compensator $G_c(s)$ is designed based on the common PI controller

$$PI = K_p + \frac{K_I}{s} = \frac{K_p \left(s + \frac{K_I}{K_p}\right)}{s} \quad (26)$$

The small signal transfer functions of the buck converter are dependent on the load condition. To eliminate the need for mode switching or gain scheduling in the controller,

control gain must ensure stability under the load conditions that place the most stringent requirements on the PI controller. If the load resistance is assumed to range from 0.25 Ω to 200 Ω , then a PI controller can be designed to satisfy both end point load conditions. Using Matlab, a range of operating conditions can be considered so that a PI controller can be produced to satisfy the requirements that the phase margin is greater than 75° and gain margin is greater than 6 dB. The zero of the PI controller is determined primarily by the light load condition, while the gain is determined primarily by the heavy load condition. Considering both, a stable controller may be found for the entire operating range. The PI controller is chosen to be

$$G_c(s) = \frac{2000(1+0.0029s)}{s} \quad (27)$$

The discrete time equivalent of $G_c(s)$ is transformed as

$$G_c(z) = G_c(s) \Bigg|_{s=\frac{2(z-1)}{T_s(z+1)}} = \frac{5.23.z - 6.59}{z - 1} \quad (28)$$

3.5. SYSTEM STABILITY ANALYSIS

The continuous time loop gain of the whole closed system, which includes the LUT and the plant, is found to be

$$T_{sys}(s) = -G_{LUT} \frac{T(s)G_c(s)}{1+T(s)G_c(s)} \quad (29)$$

G_{LUT} is the small signal gain from the LUT. From (29), the stability of the whole system depends on the gain of the LUT since the plant is designed to be stable. The IV curve of the PV module to be simulated in Section 6 is shown in Fig. 3.4 along with the corresponding G_{LUT} . From Fig. 3.5, the absolute value of the IV curve slope increases as the voltage increases, and the worst case G_{LUT} is -1.797 S. At this worst case G_{LUT} , the

loop gain of the whole closed system is shown in Fig. 3.5. As shown in Fig. 3.5, the system still has adequate gain and phase margins and is stable.

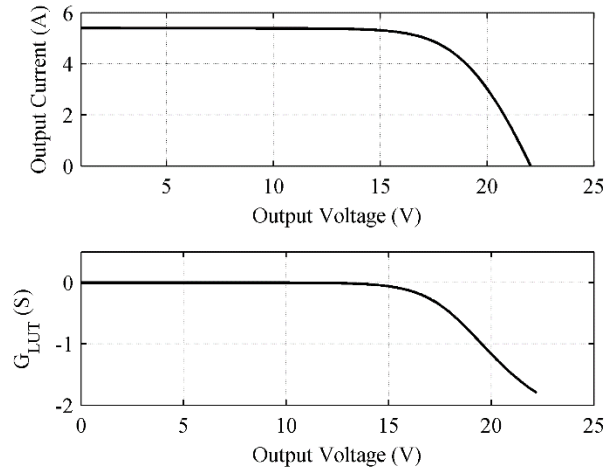


Figure 3.4. PV module IV curve and gain

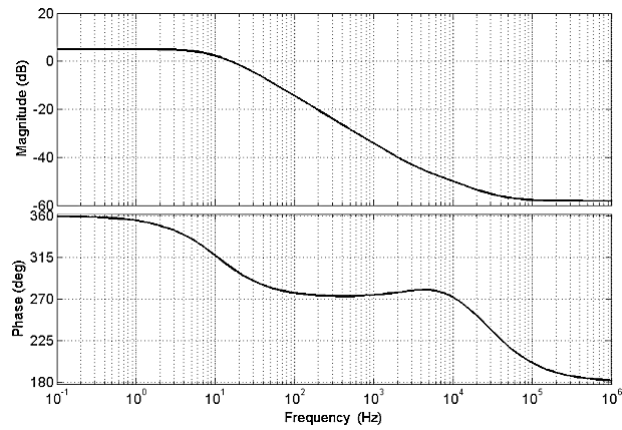


Figure 3.5. Bode plot of worst case system loop gain

4. SIMULATION RESULTS

Simulation is done in Matlab Simulink² with the help of the toolset PLECS³. The top level model schematic is shown in Fig. 4.1.

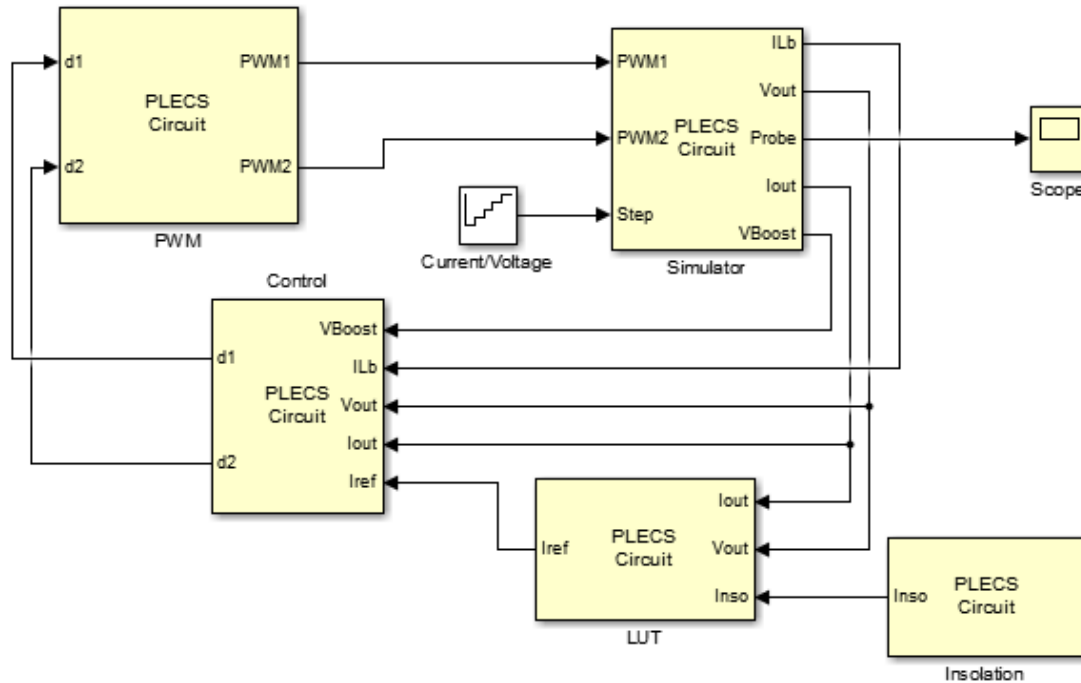


Figure 4.1. Top level schematic of the PV simulator simulation model

The “Power Stage” block shown in Fig. 4.2 houses the two stage DC-DC converter to be discussed in Section 5.

² Matlab Simulink is a registered trade mark of The Math Works, Inc.

³ PLECS is a registered trade mark of Plexim GmbH.

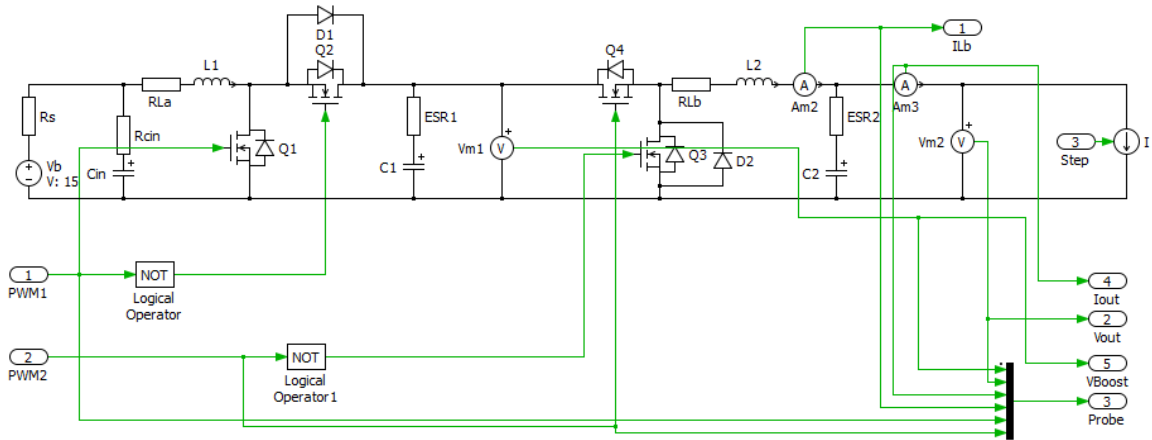


Figure 4.2. Power stage simulation model of the PV simulator

The circuit parameters used in the power stage simulation model are from those shown in Section 6 to match the experimental setup. The “IV LUT” block houses the IV curve LUT of the PV module. It is implemented through the “C-script” block available from the PLECS toolset as shown in Fig. 4.3.

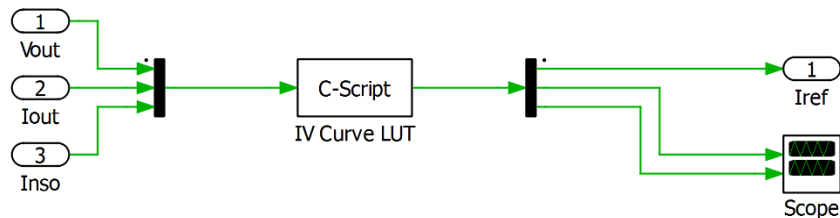


Figure 4.3. Inside of “IV LUT” block

The “C-script” block allows users to implement algorithms in C code. This greatly increases the capabilities and flexibilities of Simulink. The C code that goes in this “C-script” block can be extracted from the C codes shown in Appendix B. The “Control” block is implemented in a similar manner as shown in Fig. 4.4. The “Delay” block before the output “d2” is to simulate the zero-order hold action of a microcontroller.

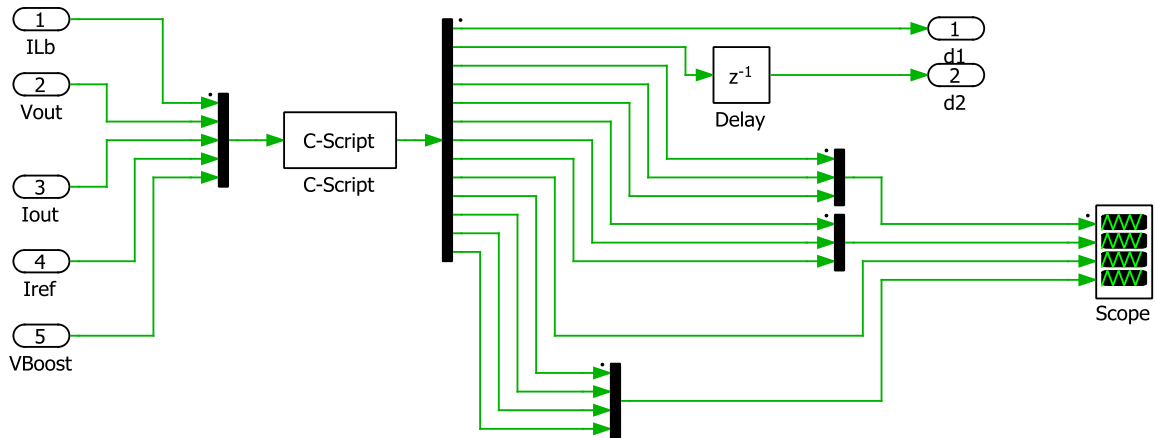


Figure 4.4. Control block simulation model for PV simulator

The steady state IV curve matching capability of the simulator is shown in Fig. 4.5 at insolation levels of 100%, 60% and 20%. The dynamic load step responses of the simulator at five different operating points with current source load is shown in Fig. 4.6. The dynamic load step responses of the simulator at five different operating points with voltage source load is shown in Fig. 4.7. The dynamic responses corresponding to insolation changes under current source load conditions are shown from Fig. 4.8 to Fig. 4.11. The dynamic responses corresponding to insolation changes under voltage source load conditions are shown from Fig. 4.12 to Fig. 4.15.

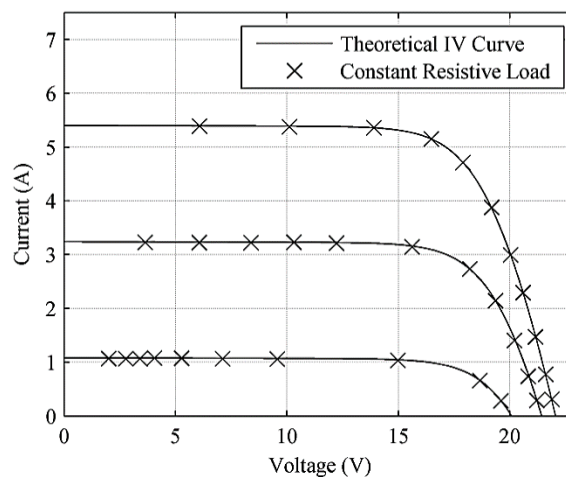


Figure 4.5. Computer Simulated performance of the PV simulator

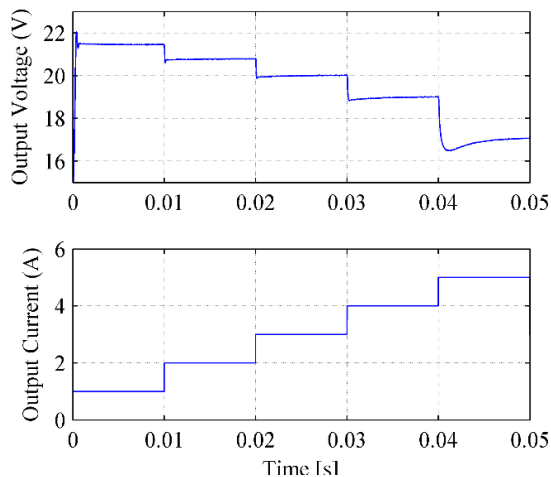


Figure 4.6 Computer Simulated output waveforms of the PV simulator when current source changes from 1A to 5A

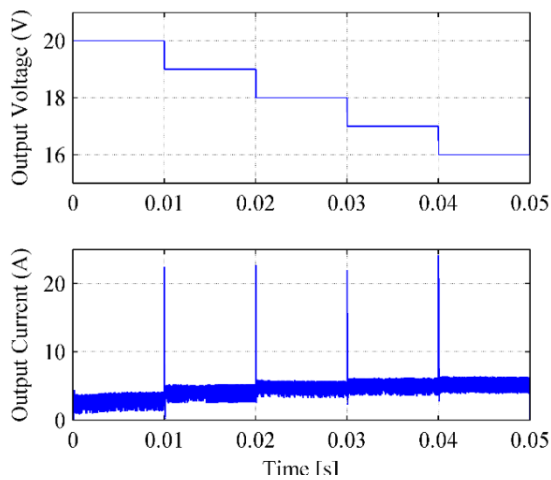


Figure 4.7 Computer Simulated output waveforms of the PV simulator when voltage source changes from 20V to 16V

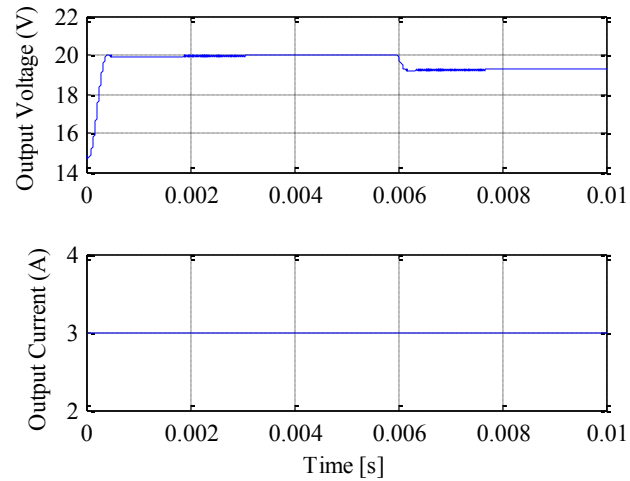


Figure 4.8 Computer Simulated insulation step change from 100% to 80% with current source load equals 3A

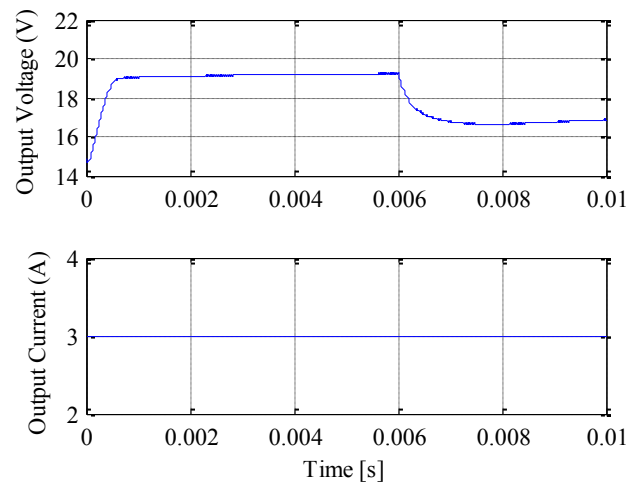


Figure 4.9 Computer Simulated insulation step change from 80% to 60% with current source load equals 3A

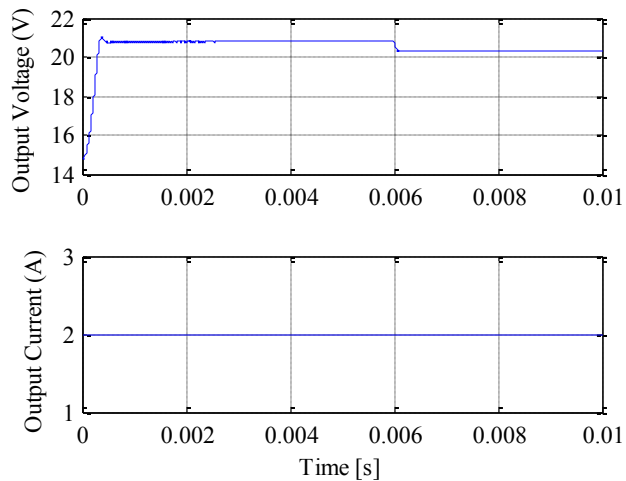


Figure 4.10 Computer Simulated insolation step change from 100% to 80% with current source load equals 2A

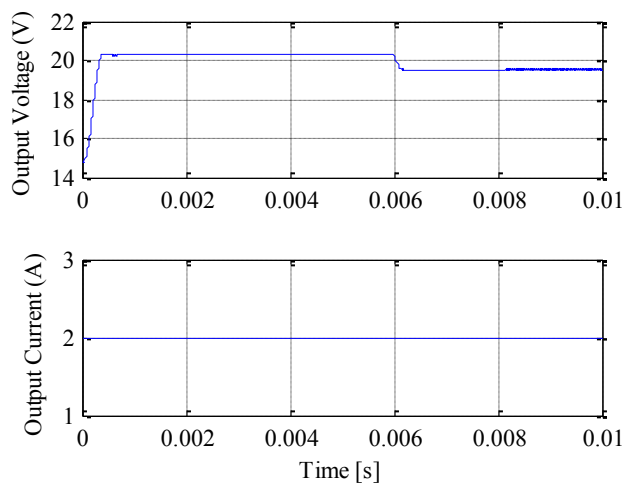


Figure 4.11 Computer Simulated insolation step change from 80% to 60% with current source load equals 2A

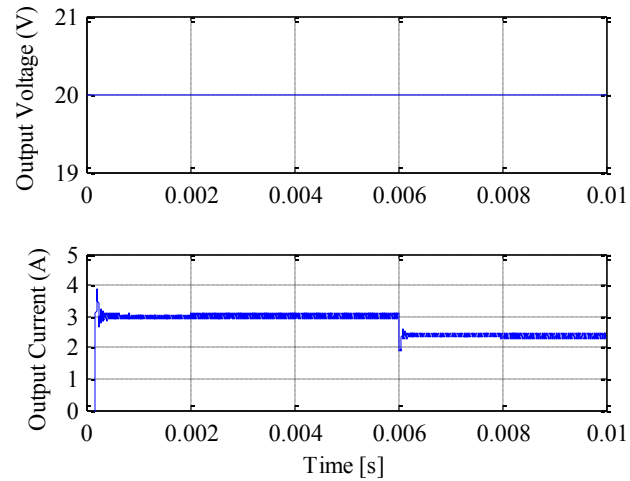


Figure 4.12 Computer Simulated insolation step change from 100% to 80% with voltage source load equals 20V

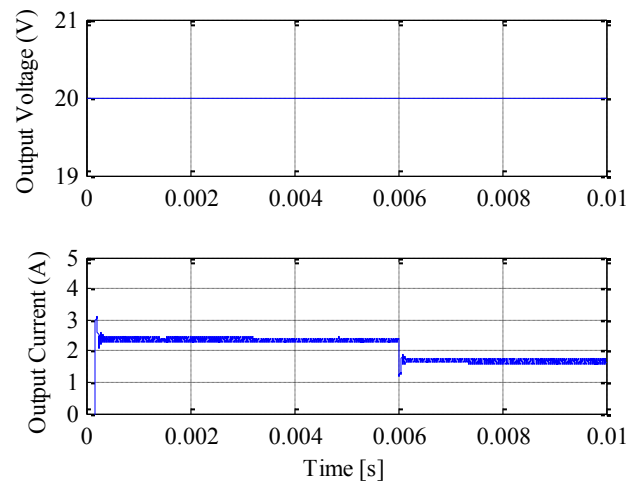


Figure 4.13 Computer Simulated insolation step change from 80% to 60% with voltage source load equals 20V

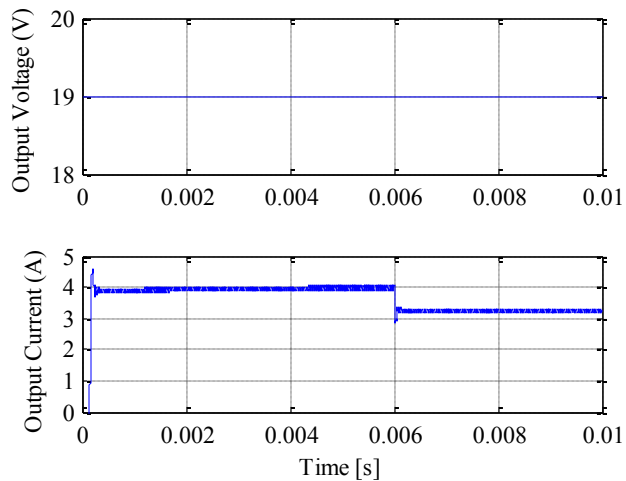


Figure 4.14 Computer Simulated insulation step change from 100% to 80% with voltage source load equals 19V

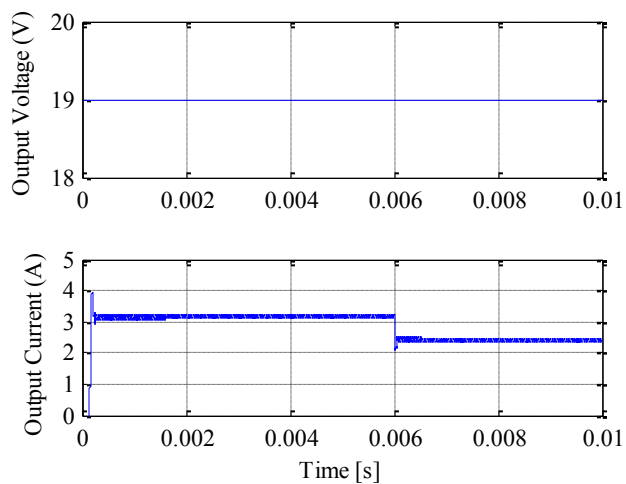


Figure 4.15 Computer Simulated insulation step change from 80% to 60% with voltage source load equals 19V

5. HARDWARE IMPLEMENTATION

5.1. POWER STAGE OF THE PV SIMULATOR

The simulator is powered by a Li-ion battery pack to create a portable device; however, it can also be powered by a fixed or programmable DC power supply when they are available. A battery or DC power supply with output voltage higher than the open circuit voltage of the PV module to be simulated might not be readily available, so a two-stage synchronous DC-DC converter is devised as shown in Fig. 5.1.

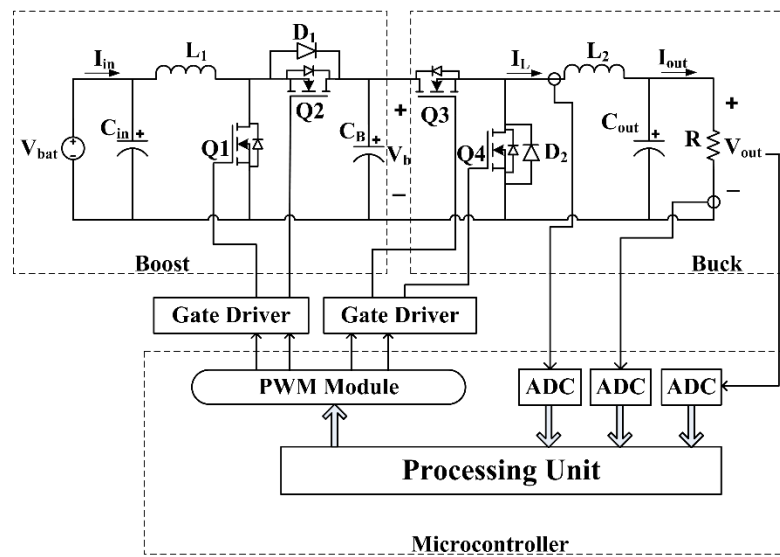


Figure 5.1. PV simulator hardware block diagram

The first stage is a step-up synchronous boost converter whose steady state output voltage is approximately

$$V_b = \frac{V_{bat}}{1 - D_b} \quad (30)$$

where V_{bat} is the input voltage from the battery or an equivalent power source, D_b is the boost converter duty ratio and V_b is the output voltage of the boost converter. For the prototype built, the boost converter outputs a nominal voltage of 30 V from a nominal

input voltage of 14.8 V from the Li-ion battery pack. The second stage is a step-down synchronous buck converter whose output voltage is approximately

$$V_{out} = D_{bk} V_b \quad (31)$$

where V_{out} is the output voltage and D_{bk} is the duty ratio of the buck converter. For the prototype built, the buck converter has an output voltage range of 0 V to 30 V from a nominal input voltage of 30 V, which means D_{bk} will range from zero to unity. One major advantage of using a synchronous topology is high efficiency, which is essential for portable applications. Another advantage of using a synchronous topology here is that the DC-DC converter will never run into DCM. This allows for a much simpler controller implementation that does not need to account for both CCM and DCM, which are qualitatively different in nature and have different dynamic models.

However, with a synchronous topology, the number of MOSFETs used is increased from two to four, which means the required number of PWM signals also increases from two to four. Dead-bands must be introduced between Q1 and Q2, and between Q3 and Q4 to prevent short-circuiting of the filter capacitor C_B due to the inherent turn-on and turn-off delays of MOSFETs. Since the source nodes of the high-side MOSFETs Q2 and Q3 have to be floating, the gate drivers must be able to provide floating gate signals to these high-side MOSFETs. In the present design, the “low and high side” gate driver IR2110 from International Rectifier is used. This type of gate driver requires that the source node of the high-side MOSFETs be connected to the drain of the low-side MOSFETs. This means that the body diodes of Q2 and Q3 will be temporarily conducting whenever Q2 and Q3 are not fully turned on and are required to conduct current. The body diode of a MOSFET is inefficient because it has comparatively high forward voltage and reverse recovery charge, so the Schottky diodes D1 and D2 are used to bypass the body diodes in Q2 and Q3 to increase efficiency.

5.2. INDUCTOR AND CAPACITOR SELECTION

The inductor current waveform of the buck converter is shown in Fig. 5.2.

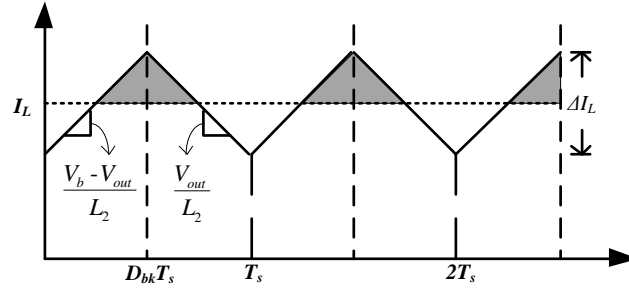


Figure 5.2. Buck converter inductor current

The ripple current then can be calculated by

$$\Delta I_L = \frac{D_{bk} T_s (V_b - V_{out})}{L_2} \quad (32)$$

where ΔI_L is the inductor peak-to-peak current ripple, and L_2 is the buck converter inductor. Substituting (31) in (32) and solving for L_2 gives

$$L_2 = \frac{V_{out} (V_b - V_{out})}{\Delta I_L f_{sw} V_b} \quad (33)$$

where f_{sw} is the switching frequency. When V_{out} is equal to half of V_b , L_2 is maximized.

This leads to

$$L_2 = \frac{V_b}{4\Delta I_L f_{sw}} \quad (34)$$

Equation (34) gives the minimum required inductance for a specified inductor peak-to-peak current ripple requirement for the proposed PV simulator. The minimum required output capacitor value to satisfy output voltage peak-to-peak ripple requirement is given as [21]

$$C_{out} = \frac{\Delta I_L}{8f_{sw} (\Delta V_{out} - R_{ESR} \Delta I_L)} \quad (35)$$

where ΔV_{out} is the peak-to-peak output voltage ripple. In the PV simulator prototype, the inductor value and capacitor value selected are to satisfy a peak-to-peak inductor current ripple of 1 A and a peak-to-peak output voltage ripple of 50 mV respectively.

Since the second stage buck converter acts as a low pass filter to the output voltage of the first stage boost converter, there is a lot of flexibility in the inductor and capacitor values for the boost converter. However, the boost converter acts as an input filter for the buck converter, so the output impedance of the boost converter must be less than the input impedance of the buck converter to ensure system stability. In order to avoid multi-stage instability, the filter capacitor C_b should be chosen to be as large as reasonable. In the PV simulator prototype, C_b is chosen to be twice as large as C_{out} , and L_1 is chosen to be the same as L_2 .

5.3. THE DSP

The DSP is required to have three ADC channels, four PWM output channels, built-in or external RAM and a processing unit, preferably with floating point math capability. The ADCs are used to measure the output voltage, output current and the buck converter inductor current, as needed by the double current mode controller. The PWM signals that go into Q1 and Q2 should run in complementary mode, which means only one MOSFET can be turned on at a time, with preset dead-band. This also applies to the PWM signals that go into Q3 and Q4. For the PV simulator prototype, the DSP chosen is the 32-bit TMS320F28335 by Texas Instrument. The DSP runs at 150MHz and has a built-in floating-point-unit, 16 channels of 12-bit ADCs, and six PWM modules, each with two PWM output channels that can run in complementary mode with preset dead-band.

6. EXPERIMENTAL RESULTS

6.1. PV SIMULATOR PROTOTYPE

The PV simulator has been built with the circuit parameters shown in Table 6.1. The physical layout of the circuit board is shown in Fig. 6.1.

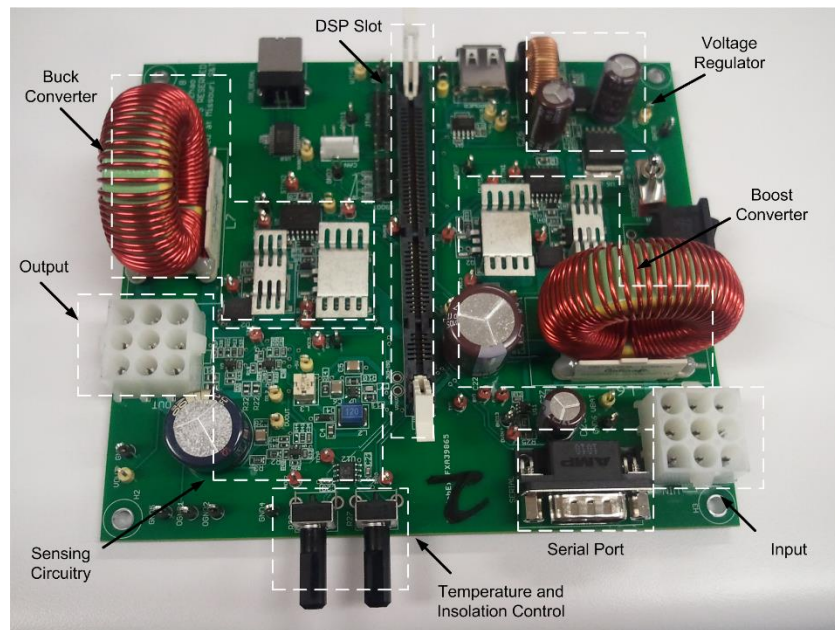


Figure 6.1. PV simulator prototype built

The main restriction to the frequency is the calculation speed of the microcontroller since it has to finish all required calculation before the next switching period starts. The PV simulator is set to simulate the multi-crystalline PV module SW-S85P from SunWize. Its datasheet parameters and the calculated parameters for the equivalent circuit model shown in Section 2 are given in Table 6.2. Note that the circuit parameters from the datasheet are taken under STC, where the temperature is 25 °C and the irradiance is 1000 W/m² (100% insolation).

Table 6.1. PV Simulator Parameter

DC-DC converter parameters	
Switching Frequency (f_{sw})	100 kHz
Inductor (L_1)	138 μ H
Inductor (L_2)	138 μ H
Inductor DC Resistance(R_{DC})	100 $m\Omega$
Input Capacitor (C_{in})	560 μ F
Filter Capacitor(C_B)	560 μ F
Output Capacitor (C_{out})	560 μ F
Output Capacitor ESR(R_{esr})	54 $m\Omega$

Table 6.2. PV Module Parameters

Datasheet Parameters (STC)	
Number of Cells in Series (N)	72
Short Circuit Current (I_{sc})	5.4 A
Open Circuit Voltage (V_{oc})	22 V
Voltage at Max. Power (V_{mpp})	17.4 V
Current at Max. Power (I_{mpp})	4.9 A
Maximum Output Power (P_{mpp})	85 W
Model Parameters	
Internal Series Resistance (R_s)	364 $m\Omega$
Internal Shunt Resistance (R_{sh})	1.21 $K\Omega$
Reverse Saturation Current (I_0)	73.42 nA
Photo-generated Current (100% Insolation) (I_{ph})	5.402 A
Ideality Factor (A)	0.6125

The outputs of the PV simulator prototype when connected to different constant current loads are shown in Fig. 6.2 for 100%, 60% and 20% insolation levels. As shown in Fig. 6.2, the output of the PV simulator prototype follows the ideal IV curves consistently without running into stability issues.

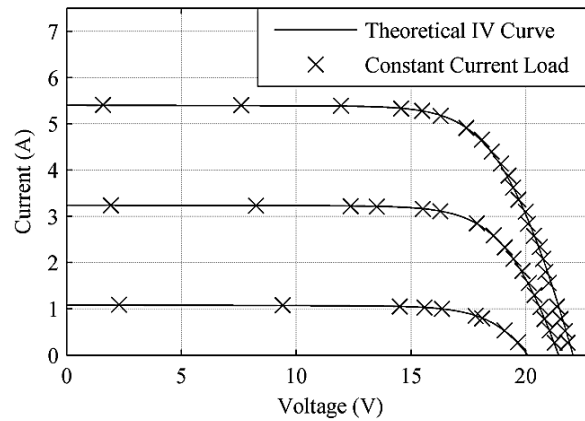


Figure 6.2. PV simulator prototype's performance

The experimental setup to test the dynamic response of the simulator is shown in Fig. 6.3, where the CH2 measures the output voltage of the PV simulator, and the CH3 measures the output current of the PV simulator. The Z_{out} is calculated by CH2 over CH3 with a switching frequency of 100 kHz. Fig. 6.4 to Fig. 6.7 show the experimental results of the PV simulator, where the top trace is the output voltage and the bottom trace is the output current. To verify theoretical results, simulations were done on a buck converter modeled in MATLAB SIMULINK software. Impedances were found by closing the voltage or current loop on the buck converter, imposing perturbations on the input voltage or load current and measuring the input and output impedances manually. The measured values were plotted on top of the theoretical impedances to compare the results. Fig. 6.8 and Fig. 6.9 show the theoretical, modeling, and measured closed-loop output impedance of the buck converter in current and voltage source loads. In each figure the blue continuous line shows the bode plot of the theoretical impedance, the x line shows the modeling output impedance, and the red dashed line shows the measured impedance from simulation. Every marker on the red dashed lines is where a measurement is done. Figure 6.8 shows the input impedance of voltage mode controlled converter and Fig. 6.9 shows the input impedance of the current mode controlled converter.

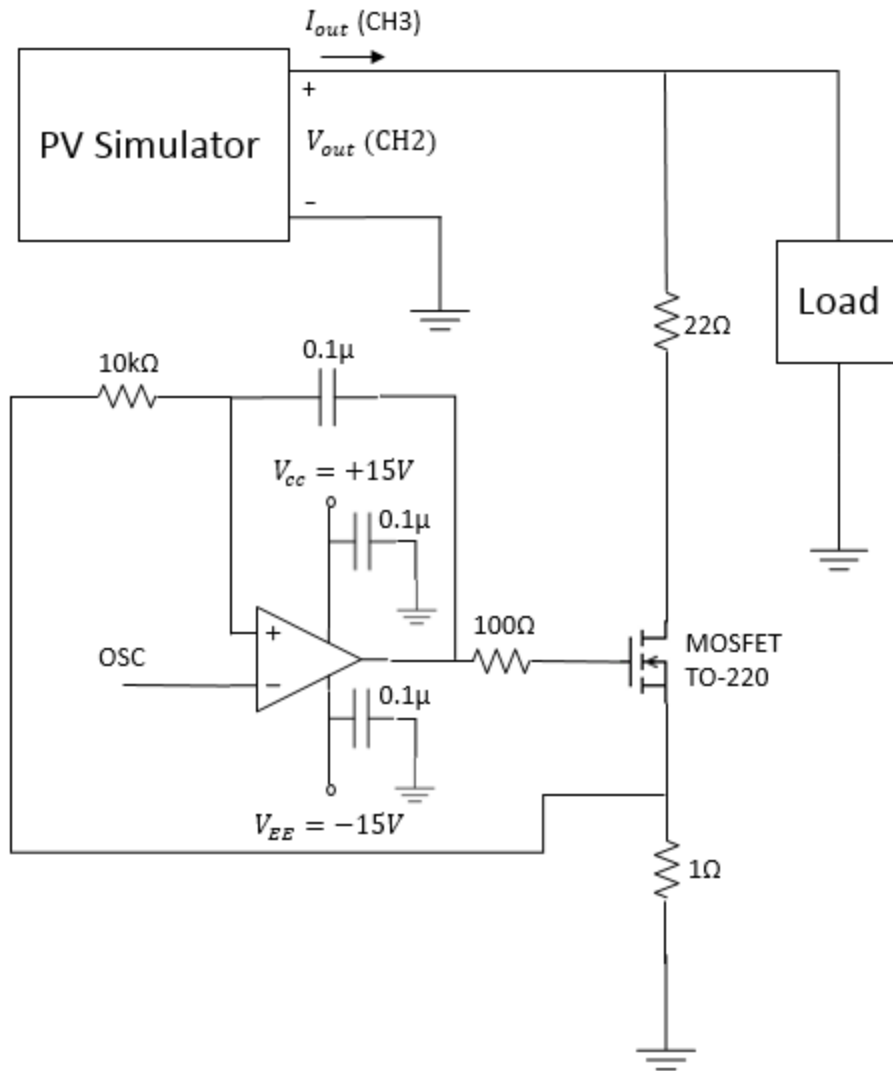


Figure 6.3. Experiment setup for the PV simulator/PV module load dynamic response

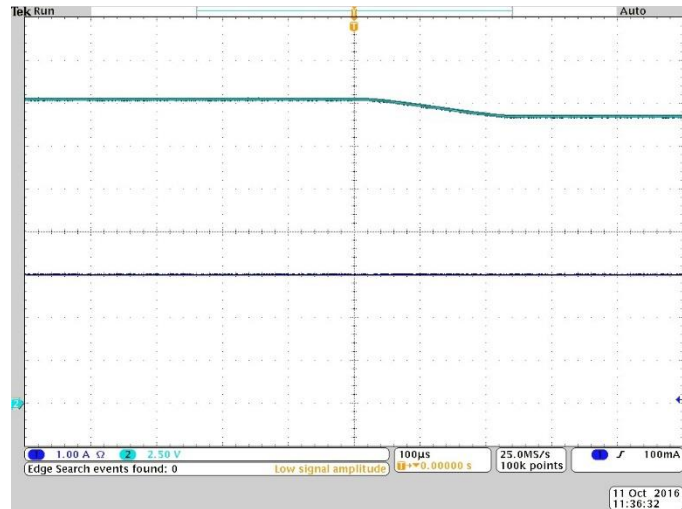


Figure 6.4. Experimental insulation step change from 100% to 80% with current source load = 3A. Upper trace: voltage, 2.5 V/div; lower trace: current, 1.0 A/div; 100 μs/div.

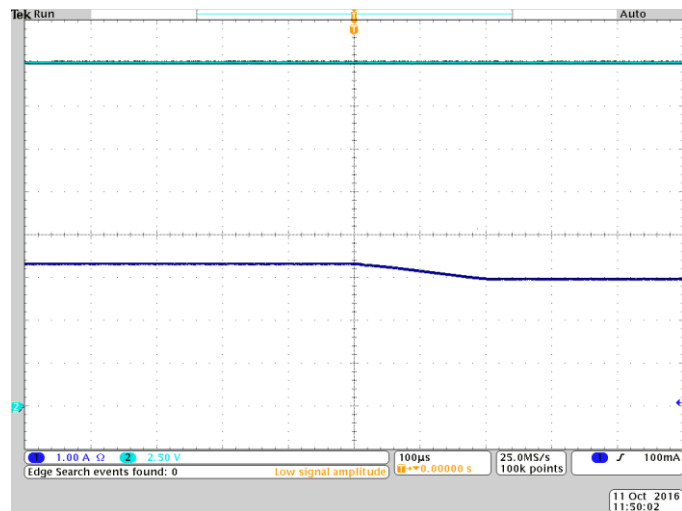


Figure 6.5. Experimental insulation step change from 100% to 80% with voltage source load = 20V. Upper trace: voltage, 2.5 V/div; lower trace: current, 1.0 A/div; 100 μs/div.

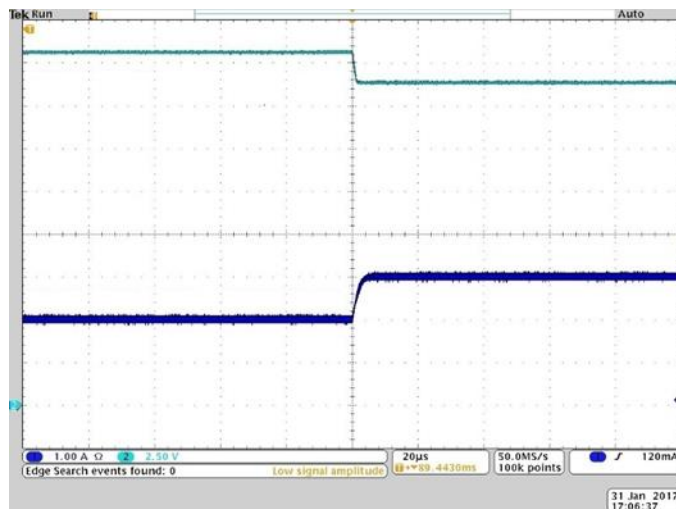


Figure 6.6. Experimental output waveforms of the PV simulator when current source changes from 2A to 3A. Upper trace: voltage, 2.5 V/div; lower trace: current, 1.0 A/div; 20 ms/div.

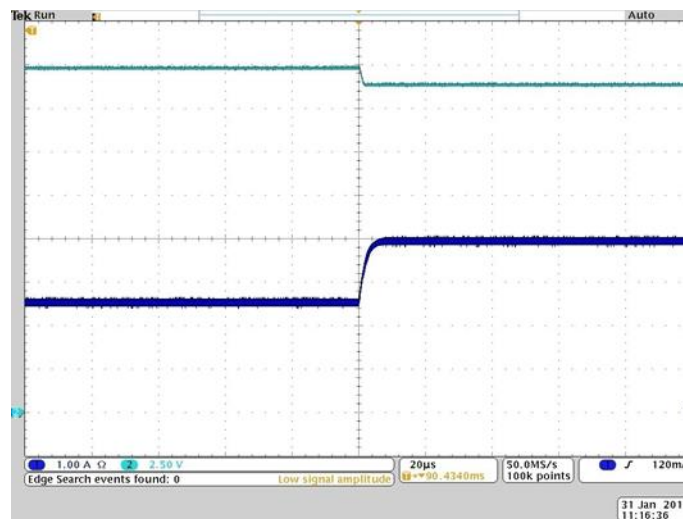


Figure 6.7. Experimental output waveforms of the PV simulator when voltage source changes from 20V to 19V. Upper trace: voltage, 2.5 V/div; lower trace: current, 1.0 A/div; 20 μs/div.

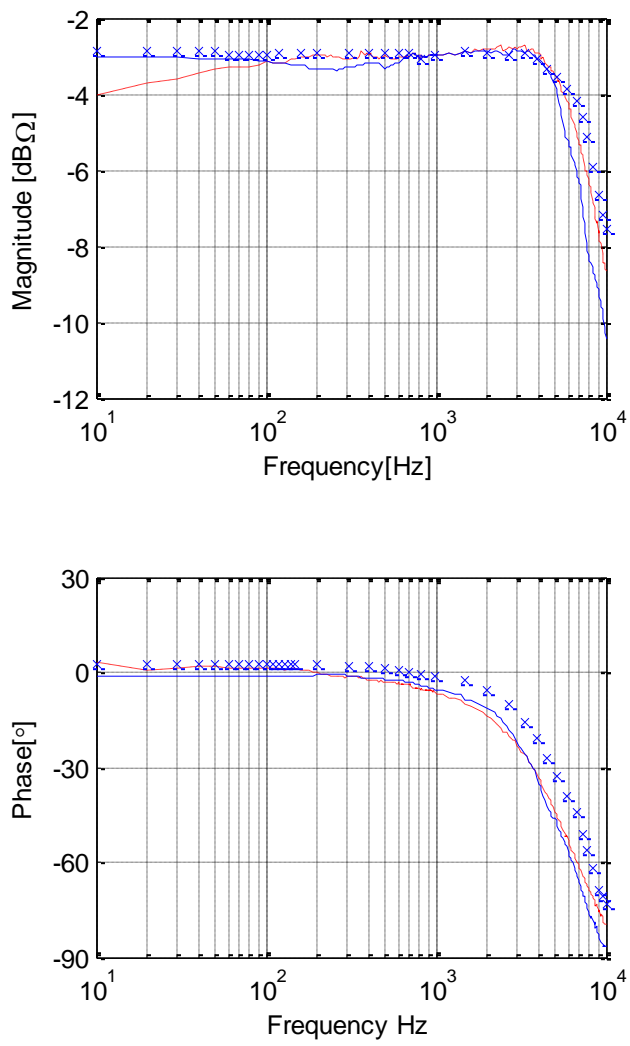


Figure 6.8. Theoretical, modeling, and measured closed-loop output impedances of buck converter in current source load. The red dashed line traces show the simulation results, the x line show the modeling output impedance, and the blue solid traces show the measured impedance.

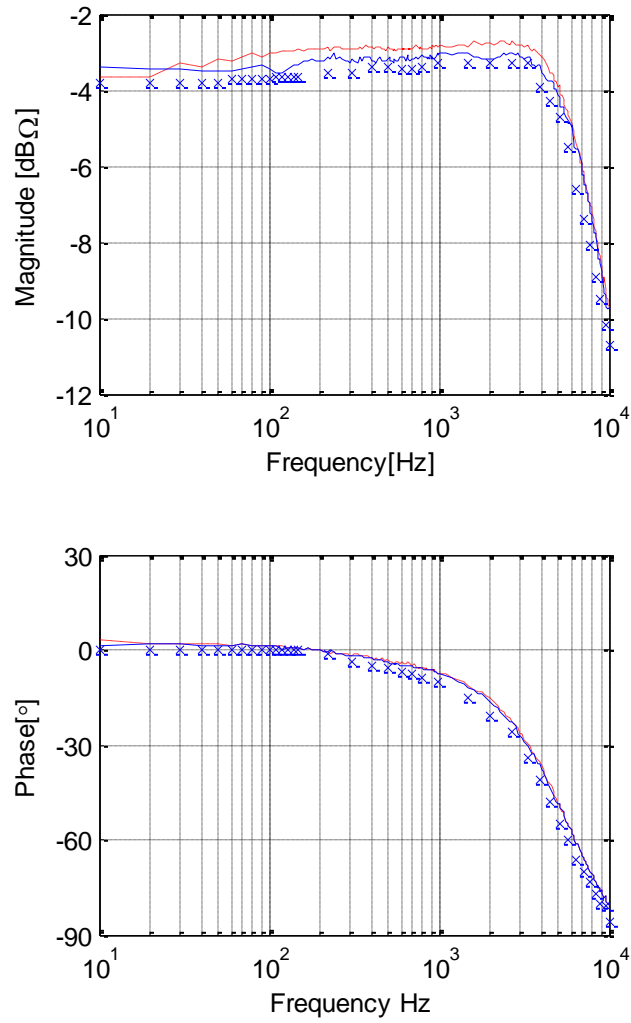


Figure 6.9. Theoretical, modeling, and measured closed-loop output impedances of buck converter in voltage source load. The red dashed line traces show the simulation results, the x line show the modeling output impedance, and the blue solid traces show the measured impedance.

7. CONCLUSION

7.1. RESEARCH FINDINGS

This thesis presents a digitally implemented PV simulator which consists of a DC-DC converter and a DSP. The IV characteristic of the PV module of interest is implemented as a LUT that resides in the RAM of a microcontroller. A double current mode controller that consists of a PI controller and a predictive current mode controller is used to regulate the output current of the DC-DC converter to match the IV curve in the LUT. With a double current mode controller, the stability of the system is guaranteed over a wide range of load conditions. A portable PV simulator prototype of 85 Watts is built to demonstrate the effectiveness of the presented method. It is shown that the prototype has excellent IV curve matching capability, and it can be perturbed, as by a MPPT controller, with a sampling frequency of up to 2 kHz. The dynamic response of the physical PV module of interest is also examined, and it has a maximum settling time of approximately 5 μ s, which translates to a maximum sampling frequency of 200 kHz. It is observed that the settling time of the PV simulator prototype is significantly more than the settling time of a real PV module. The effectiveness of the PV simulator prototype hence is dependent on the MPPT algorithm and its sampling frequency. Even though the PV simulator prototype falls short of the step response of a real PV module, this gap can be bridged by better component selection and faster microcontrollers.

7.2. FUTURE WORK

It is possible to improve the dynamic response of the simulator prototype by reducing the size of the output capacitor while at the same time satisfying the output voltage ripple requirement. For a fixed switching frequency, the selection of the output capacitor for the simulator prototype is dominated by the ESR, so the best way to reduce the size of the output capacitor is to replace it with a capacitor of a different material, such as Polymer Aluminum, which has lower ESR than Aluminum Electrolytic capacitors. Another way to reduce the size of the output capacitor is to reduce the inductor ripple by using large inductor values. However, larger inductor values mean lower rate of change of the inductor current, which could limit the system bandwidth. A

method to balance inductor and capacitor values to achieve maximum system bandwidth is of great value here. The last method to reduce the size of the output capacitor is to increase the switching frequency. However, higher frequency requires faster processors, better power management for the DC-DC converter and capacitors that are suitable for high frequency operation.

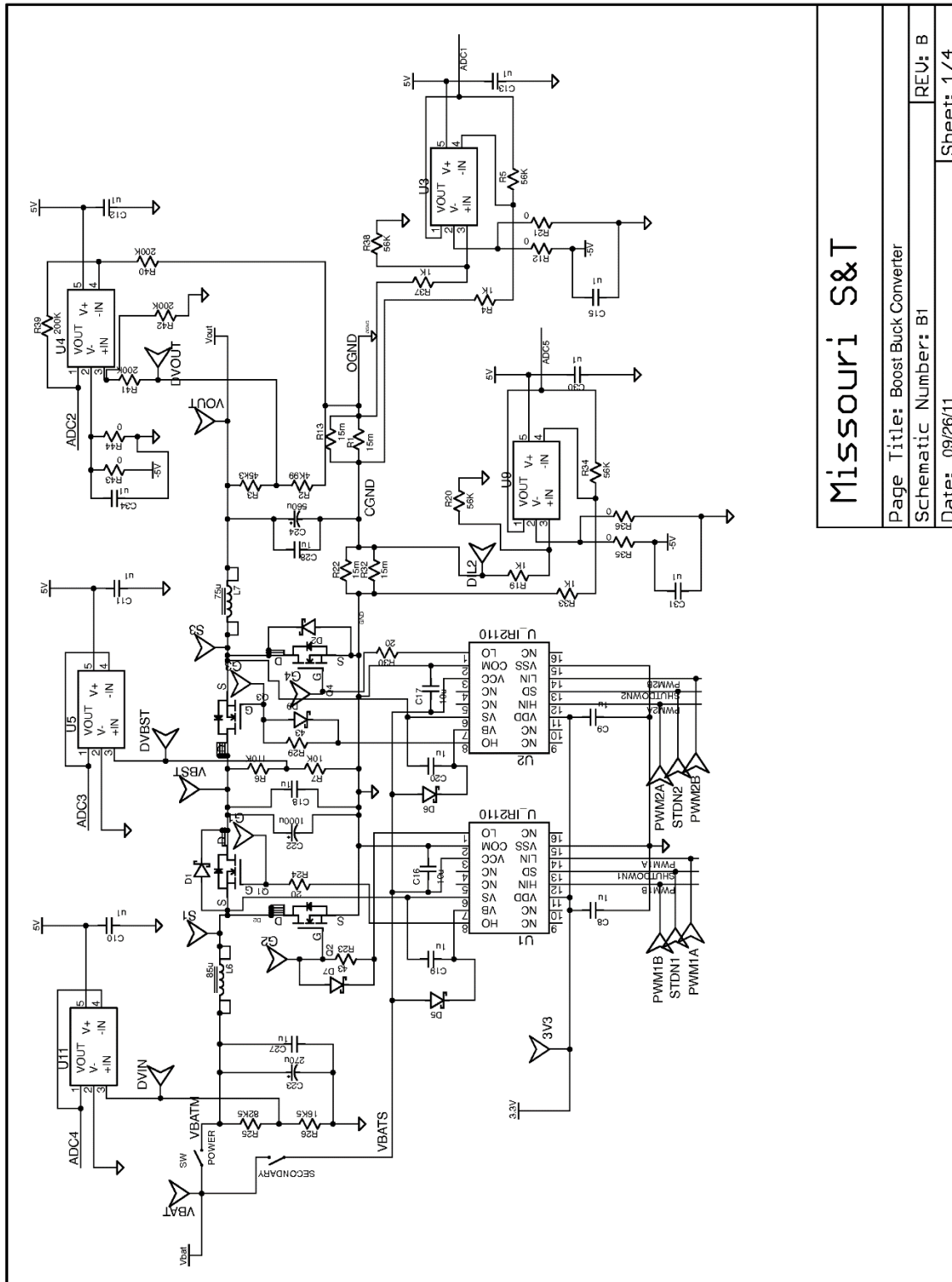
It is also beneficial to see if multiple PV simulators can be connected in a series or parallel configuration to enable emulation of higher power PV modules. This would greatly increase the flexibility of the PV simulator and give reasons for the mass production of a PV simulator of low output power, such as the prototype built.

A computer user interface, such as a graphic user interface or a command prompt, needs to be designed to let users input all the parameters about the PV module of interest and the environmental conditions of the simulation in order to run the PV simulator prototype in stand-alone mode. There is a serial port built into the PV simulator prototype, which is connected to the SCI channels of the DSP. This port will be connected to the RS-232 serial port of a computer. There is also a USB interface for the SCI of the DSP for computers that don't have serial ports, as it is true for most modern computers.

APPENDIX A.
PRINTED CIRCUIT BOARD DESIGN

This appendix contains the EAGLE⁴ schematics and printed circuit board (PCB) physical layout information for the photovoltaic simulator prototype built. Figures A.1 through A.4 show the schematics for the PV simulator prototype. The PCB consists of two layers and utilizes the ground plane construct technique. Figure A.5 and A.6 show the PCB physical top and bottom board layer of the PV simulator prototype. In the physical board layout, circles represent vias or through holes, and the dashed lines specify the ground plane borders.

⁴ The EAGLE logo is a registered trademark of CadSoft Computer.



Missouri S&T

Page Title: Boost Buck Converter

Schematic Number: B1

Date: 09/26/11

REV: B

Sheet: 1/4

Figure A.1. PV simulator PCB schematic sheet one

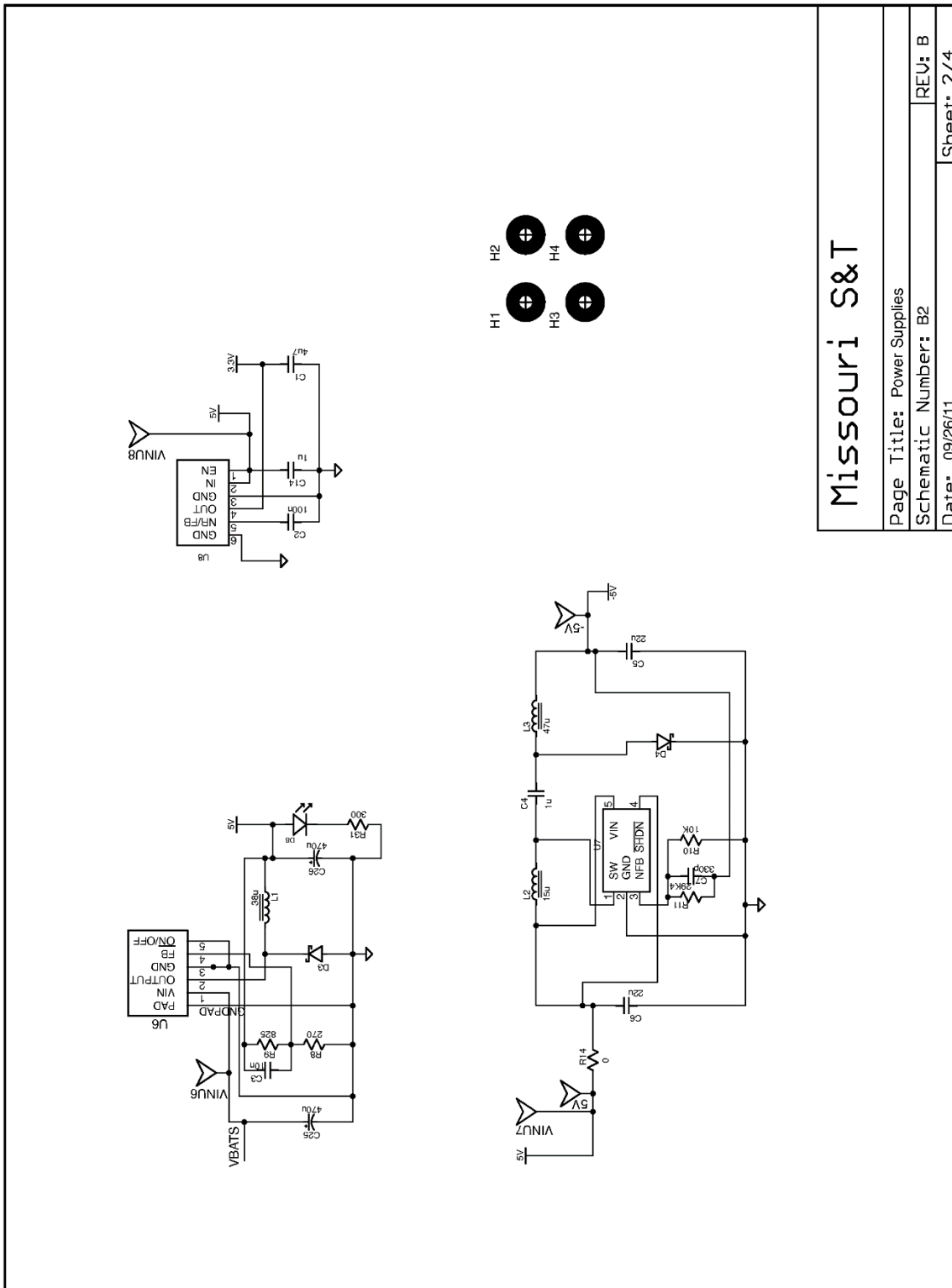


Figure A.2. PV simulator PCB schematic sheet two

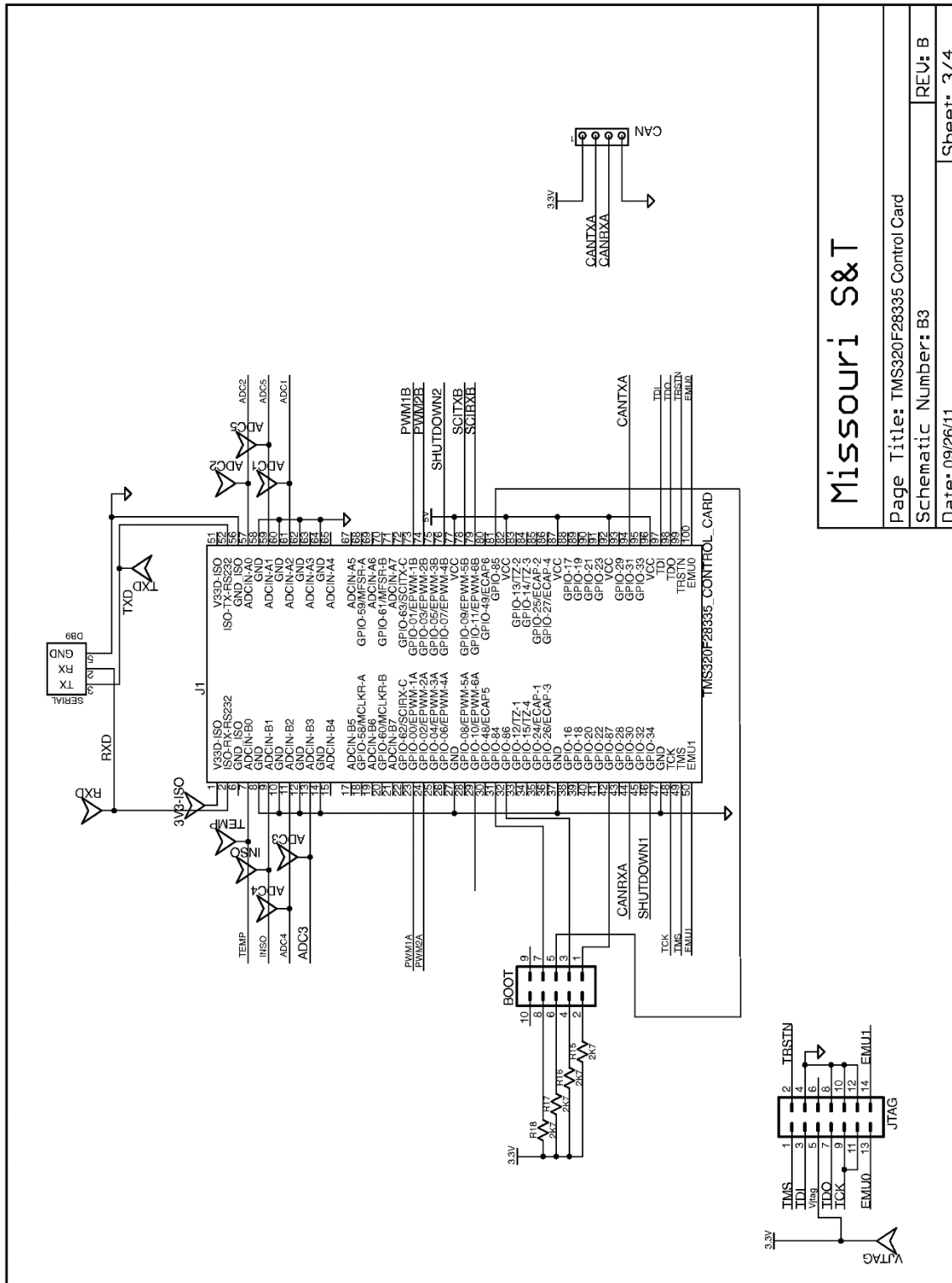
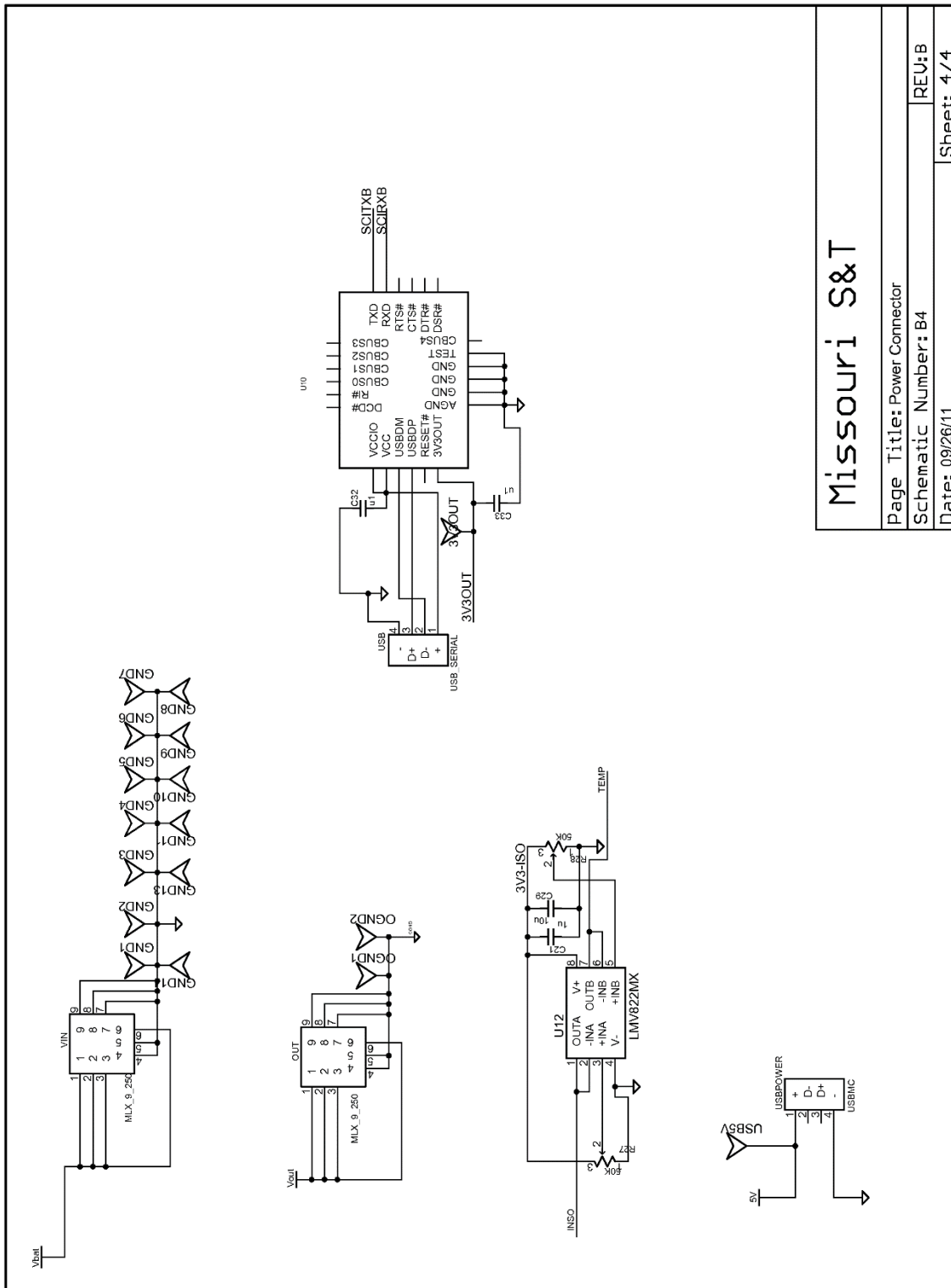


Figure A.3. PV simulator PCB schematic sheet three



Missouri S&T

Page Title: Power Connector	
Schematic Number: B4	
Date: 09/26/11	
REU:B	Sheet: 4/4

Figure A.4. PV simulator PCB schematic sheet four

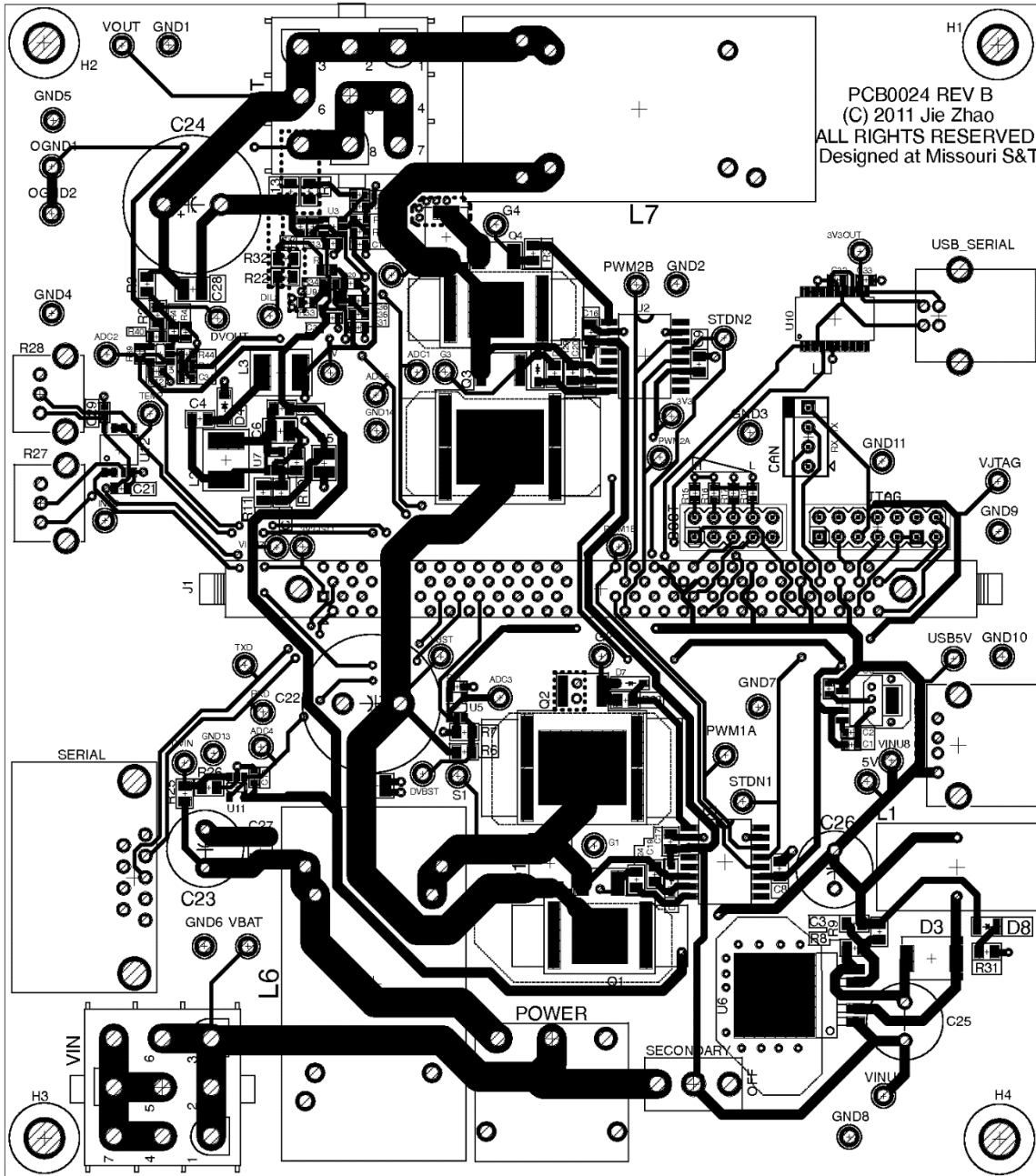


Figure A.5. Top layer of board physical layout

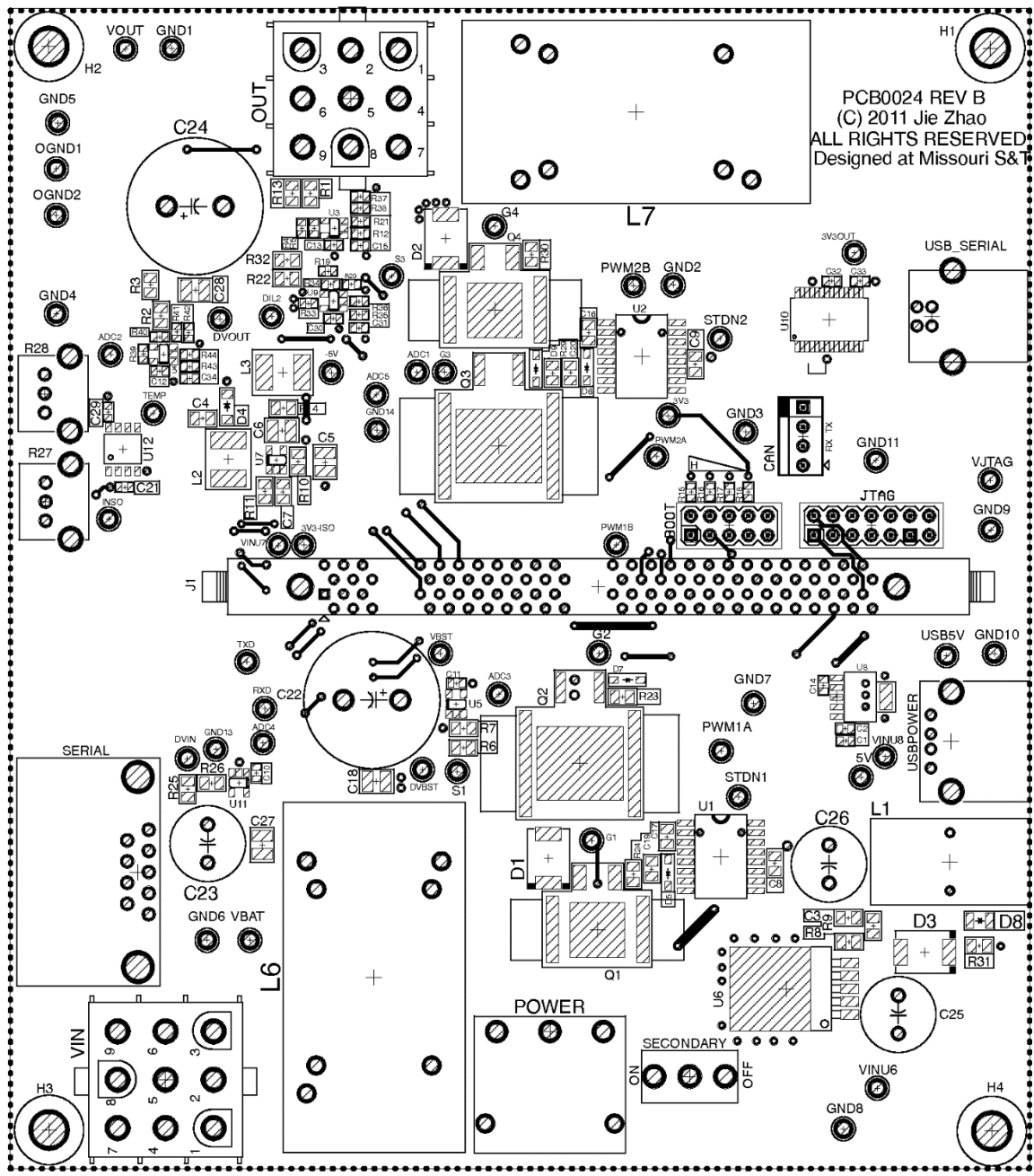


Figure A.6. Bottom layer of board physical layout

APPENDIX B.
MATLAB CODE TO EXTRACT PV MODULE MODEL PARAMETERS

This appendix contains the Matlab code to implement the photovoltaic module equivalent circuit model parameter extraction method shown in Section 3.1. The solar panel parameters used is for the PV module SW-S85P from Sunwize, and the extracted parameters are shown in Table 6.2; however, users can modify the solar panel datasheet parameters to extract equivalent model parameters for any type of PV module.

```

%% Extraction of PV module parameters based on datasheet values
% PV Module SW-S85P from SunWire

close all;
clear all;

% Intitalize parameters-----
A=1;           % initial ideality factor
k=1.38e-23;    % Boltzman's Constant
q=1.1602e-19;  % elemental charge
Tstc=300;      % STC temperature
Io=1;         % initial dark saturation current
Iph=0;        % initial photo generated current
Rs=0;         % initial series resistance
Rsh=1000;     % initial shunt resistance
Vt=.026;     % initial thermal voltage

% solar panel datasheet parameters-----
n=72;         % number of panels
Voc=22;       % open circuit voltage
Isc=5.4;      % short circuit current
Impp=4.9;     % max power point current
Vmpp=17.4;    % max power point voltage

% Test values of Rs and Rsh-----
Rs_t=zeros(1,3000);
Rsh_t=zeros(1,3000);
for i=1:1:length(Rs_t) % Initialize test values
    Rs_t(i)=.5 * power(.9995,i);
    Rsh_t(i)=5000 * power(.9995,i);
end

% helper values-----
dpdvtemp=0;
dpdv=0;
didvtemp=0;
didv=0;
count=1;

% Numeric iteration method of extracting the PV panel model parameters
% with the method presented in "PV panel model based on datasheet
values"
% by D. Sera etc.
for i=1:1:length(Rs_t)
    Rs=Rs_t(i);
    for j=1:1:length(Rsh_t)
        Rsh=Rsh_t(j);
        Vt=(Vmpp+Impp*Rs-Voc)/n/log((Isc-(Vmpp+Impp*Rs-
Isc*Rs)...
        /Rsh-Impp)/(Isc-(Voc-Isc*Rs)/Rsh));
        alpha=(Isc*Rsh-Voc+Isc*Rs)...
        *exp((Vmpp+Impp*Rs-Voc)/n/Vt)/(n*Vt);
        dpdv=Impp+Vmpp*((-1*alpha/Rsh-
1/Rsh)/(1+alpha/Rsh+Rs/Rsh));
    end
end

```

```

        if (imag(Vt)~=0 || Vt<=0)
            continue;
        elseif (dpdv==0)
            break;
        elseif (sign(dpdvtemp)*sign(dpdv)==-1)
            break;
        else
            dpdvtemp=dpdv;
        end
    end
    beta=(Isc*Rsh-Voc+Isc*Rs)*exp((Isc*Rs-Voc)/n/Vt)/(n*Vt);
    didv=(-1*beta/Rsh-1/Rsh)/(1+beta/Rsh+Rs/Rsh)+1/Rsh;
    if (didv==0)
        break;
    end
    if (sign(didvtemp)*sign(didv)==-1)
        break;
    else didvtemp=didv;
    end
end

% Outputs the finalized parameters-----
Vt
Rs
Rsh
Io=(Isc-(Voc-Isc*Rs)/Rsh)*exp(-1*Voc/n/Vt)
Iph=Io*exp(Voc/n/Vt)+Voc/Rsh
A=Vt*q/k/Tstc

```


BIBLIOGRAPHY

- [1] J. W. Kimball and P. T. Krein, "Discrete-time ripple correlation control for maximum power point tracking," *IEEE Trans. Power Electron.*, vol. 23, pp. 2353-2362, Sep. 2008.
- [2] T. Esumi and P. L. Chapman, "Comparison of photovoltaic array maximum power point tracking techniques," *IEEE Trans. Energy Conversion*, vol. 22, pp. 439-449, June 2007.
- [3] H. Nagayoshi, "Characterization of the module/array simulator using I-V magnifier circuit of a pn photo-sensor " in *Proc. 3rd World Conf. Photovoltaic Energy Conversion*, 2003, vol. 2, pp. 2023-2026.
- [4] A. Koran, K. Sano, R. Y. Kim, and J. S. Lai, "Design of a photovoltaic simulator with a novel reference signal generator and two-stage LC output filter," *IEEE Trans. Power Electron.*, vol. 25, pp. 1331-1338, May 2010.
- [5] G. Vachtsevanos and K. Kalaitzakis, "A hybrid photovoltaic simulator for utility interactive studies," *IEEE Trans. Energy Conversion*, vol. EC-2, pp. 227-231, June 1987.
- [6] E. Koutroulis, K. Kalaitzakis, and V. Tzitzilonis, "Development of a FPGA-based system for real-time simulation of photovoltaic modules," in *Proc. IEEE RSP'06*, 2006, pp. 200-206.
- [7] H. Lee, M. J. Lee, S. N. Lee, H. C. Lee, H. K. Nam, and S. J. Park, "Development of photovoltaic simulator based on DC-DC converter," in *Proc. 31st INTEL 2009*, 2009, pp. 1-5.
- [8] J. P. Lee, B. D. Min, T. J. Kim, *et al.*, "Development of a photovoltaic simulator with novel simulation method of photovoltaic characteristics," in *Proc. 31st INTEL 2009*, 2009, pp. 1-5.
- [9] Y. Li, T. Lee, and F. Z. Peng, "A hybrid control strategy for photovoltaic simulator," in *Proc. IEEE APEC 2009*, 2009, pp. 899-903.
- [10] M. C. D. Piazza, M. Pucci, A. Ragusa, and G. Vitale, "Analytical versus neural real-time simulation of a photovoltaic generator based on a DC-DC converter," *IEEE Trans. Industry Applications*, vol. 46, pp. 2501-2510, Dec 2010.
- [11] S. Chattopadhyay and S. Das, "A digital current-mode control technique for DC-DC converters," *IEEE Trans. Power Electron.*, vol. 21, pp. 1718-1726, Nov. 2006.

- [12] J. Chen, A. Prodic, R. W. Erickson, and D. Maksimovic, "Predictive digital current programmed control," *IEEE Trans. on Power Electron.*, vol. 18, pp. 411-419, Jan 2003.
- [13] Y. S. Lai and C. A. Yeh, "Predictive digital-controlled converter with peak current-mode control and leading-edge modulation," *IEEE Trans. on Ind. Electron.*, vol. 56, pp. 1854-1863, June 2009.
- [14] S. Bibian and H. Jin, "Time delay compensation of digital control for DC switchmode power supplies using prediction techniques," *IEEE Trans. Power Electron.*, vol. 15, pp. 835-842, Sep. 2000.
- [15] S. Bibian and H. Jin, "High performance Predictive dead-beat digital controller for DC power supplies," *IEEE Trans. Power Electron.*, vol. 17, May 2002.
- [16] P. Athalye, D. Maksimovic, and R. Erickson, "Variable-frequency predictive digital current mode control," *IEEE Power Electron. Letters*, vol. 2, pp. 113-116, Dec. 2004.
- [17] E. Lorenzo, G. Araujo, A. Cuevas, M. Egido, J. Minano, and R. Zilles, *Solar electricity: engineering of photovoltaic system*. Seville, Spain: Progensa, 1994.
- [18] D. A. Neaman, *Microelectronics Circuit Analysis and Design*, 3 ed. New York: McGraw-Hill, 2007.
- [19] D. Sera, R. Teodorescu, and P. Rodriguez, "PV panel model based on datasheet values," in *Proc. IEEE ISIE 2007*, 2007, pp. 2392-2396.
- [20] J. Stewart, *Calculus*, 5th ed: Thompson, 2003.
- [21] R. W. Erickson and D. Maksimovic, *Fundamentals of Power Electronics*, 2 ed: Kluwer, 2004.

VITA

Weichao Zhang was born in Guangzhou, Guangdong, China. He came to the United States in 2009. He received the Bachelor of Science degree in Electrical Engineering from Missouri University of Science and Technology in 2014 and the Master of Science degree in Electrical Engineering from Missouri University of Science and Technology in May 2017.